The balance between Cathepsin C and Cystatin F controls remyelination in the brain of *Plp1*-overexpressing mouse, a chronic demyelinating disease model.

Takahiro Shimizu[1,2,8], Wilaiwan Wisessmith[1,2,5], Jiayi Li[2,3], Manabu Abe[4], Kenji Sakimura[4], Banthit Chetsawang[5], Yoshinori Sahara[9], Koujiro Tohyama[7,9], Kenji F. Tanaka[2,6], and Kazuhiro Ikenaka[2,3]

1 These authors contributed equally.

2 Division of Neurobiology and Bioinformatics, National Institute for Physiological Sciences, Okazaki, Japan.

3 Department of Physiological Sciences, Graduate University for Advanced Studies (SOKENDAI), Okazaki, Japan.

4 Brain Research Institute, Niigata University, Niigata, Japan.

5 Research Center for Neuroscience, Institute of Molecular Biosciences, Mahidol University, Salaya, Nakhonpathom, Thailand.

6 Department of Neuropsychiatry, Keio University, Tokyo, Japan.

7 Center for Electron Microscopy and Bio-Imaging Research, Iwate Medical University, Iwate, Japan

8 (Current affiliation): Wolfson Institute for Biomedical Research, University College London, London, United Kingdom.

9 Department of Physiology, Iwate Medical University School of Dentistry, Iwate, Japan.

Correspondence should be addressed to: Kazuhiro Ikenaka, 5-1 Aza-Higashiyama, Myodaiji, Okazaki, Aichi, Japan 444-8787. Telephone number: +81-564-59-5245.

E-mail address: ikenaka@nips.ac.jp

Running title

CatC and CysF regulate remyelination

Title page: 163 words

Running title: 36 characters

Main points:247 characters

Key words: 68 characters

Abstract: 152 words

Introduction: 955 words

Materials and methods: 1409 words

Results: 2169 words

Discussion: 852 words

Acknowledgements: 191 words

References: 1511 words

Figure legends: 1224 words

Figure number: 9 figures and 2 supplementary

Total word count: 8626 words

Main points

-- The balance between cystatin F (CysF) and cathepsin C (CatC) regulates remyelination in a mouse model of demyelinating disease.

-- CysF and CatC knockdown, and CatC overexpression in microglia were generated using a versatile gene manipulation system.

Keywords

Demyelination, remyelination, microglia, cysteine protease inhibitor

The authors have no conflicts of interest to declare.

Abstract

In demyelinating diseases such as multiple sclerosis (MS), an imbalance between the demyelination and remyelination rates underlies the degenerative processes. Microglial activation is observed in demyelinating lesions; however, the molecular mechanism responsible for the homeostatic/environmental change remains elusive. We previously found that cystatin F (CysF), a cysteine protease inhibitor, is selectively expressed in microglia only in actively demyelinating/remyelinating lesions but ceases expression in chronic lesions, suggesting its role in remyelination. Here we report the effects of manipulating the expression of CysF and cathepsin C (CatC), a key target of CysF, in a murine model of transgenic demyelinating disease, $Plp^{4e/-}$. During the active remyelinating phase, both CysF knockdown (CysFKD) and microglial-selective CatC overexpression (CatCOE) showed a worsening of the demyelination in $Plp^{4e/-}$ transgenic mice. Conversely, during the chronic demyelinating phase, CatC knockdown (CatCKD) ameliorated the demyelination. Our results suggest that the balance between CatC and CysF expression controls the demyelination and remyelination process.

Introduction

In multiple sclerosis (MS), the immune system attacks the myelin sheath causing inflammation and injury to the sheath, and ultimately to the nerve fibers that it surrounds. This results in numerous sclerotic regions and the appearance of naked axons where premyelinating oligodendrocytes failed to remyelinate the axons. It has become increasingly important to elucidate the causes of this impaired remyelination in order to aid the development of a treatment for chronic MS lesions. An imbalance in the demyelination/remyelination rate underlies the degenerative processes in demyelinating lesions. By investigating the environmental cues associated with this imbalance, insights into means of limiting demyelination and promoting remyelination may be obtained. It was originally proposed that the main cause of impaired remyelination was the lack of oligodendrocyte progenitor cells (OPCs). However, premyelinating oligodendrocytes and OPCs have been found in demyelinated MS lesions (Chang et al., 2000; Chang et al., 2002) and in mice with experimental autoimmune encephalomyelitis (EAE) (Girolamo et al., 2011). Moreover, we have shown that additional oligodendrocyte lineage cells are produced during repair, but in chronic demyelinated lesions their processes degenerate after maturation (Shimizu et al., 2013).

Thus, in chronic demyelinated lesions the environment surrounding oligodendrocytes and OPCs likely changes from being one that is permissive to remyelination to one that is non-permissive. The significance of the environment surrounding oligodendrocytes and OPCs has been gaining increased attention due to the identification of factors such as PSA-NCAM (Charles et al., 2002) and hyaluronan (Back et al., 2005) that inhibit remyelination.

Microglia are well known to act as innate resident immune cells and active surveyors of the extracellular environment in the central nervous system (CNS) (Arnoux and Audinat, 2015; Kreutzberg, 1996; Ransohoff and Perry, 2009; Schafer et al., 2012; Shemer et al.,

2015). During the remyelination process, microglia play a critical role in myelin removal (Kotter et al., 2006). However, it has been reported that microglial paralysis can repress experimental autoimmune encephalomyelitis (EAE) (Heppner et al., 2005). Moreover, it is known that macrophages laden with myelin are anti-inflammatory in MS (Boven et al., 2006), and that myelin-phagocytosing macrophages in the CNS and the peripheral nervous system (PNS) show both inflammatory and anti-inflammatory responses (van Rossum et al., 2008). Also, CCR5 expression on microglia is associated with early remyelination (Trebst et al., 2008). Thus, the comprehensive role of microglia in remyelination remains elusive.

We have utilized the hemizygous proteolipid protein 1 (*Plp1*) transgenic mouse strain, 4e ($Plp^{4e/-}$), which has two extra *Plp1* genes, and demonstrated its use as an ideal model for studying demyelination and remyelination (Kagawa et al., 1994; Shimizu et al., 2013). The use of appropriate animal models is essential for studying the mechanisms underlying these environmental changes. Transgenic $Plp^{4e/-}$ mice appear to undergo normal myelination with no signs of myelin degeneration until two months of age. However, at two months of age they show spontaneous demyelination accompanied by remyelination in the early phase but which terminates after 6 months of age (during the chronic demyelinating phase), resulting in the appearance of chronic lesions throughout the central nervous system and naked axons (Kagawa et al., 1994). During the demyelinating phase, $Plp^{4e/-}$ mice do not show T-cell infiltration in the lesions. However, an upregulation of *IL-1*β and *TNF-*α mRNA was detected, although their protein levels were below detection (unpublished data). While the oligodendrocytes extended processes parallel with the axons, they failed to form myelin structure, indicative of the presence of premyelinating oligodendrocytes (Ma et al., 2006). The presence of premyelinating oligodendrocytes in chronic demyelinated lesions is also associated with MS (Chang et al., 2002). Thus, we used the $Plp^{4e/-}$ mouse as a model to study the mechanisms behind remyelination impairment in chronic lesions.

In a previous study, we performed cDNA microarray analysis using *Plp*$^{4e/-}$ mice to search for changes in gene expression (Ma et al., 2007). We identified that microglial CysF expression is indicative of ongoing demyelination/remyelination and the absence of CysF expression indicates the cessation of remyelination in demyelinating lesions (Ma et al., 2011). Cystatin F is a cysteine protease inhibitor expressed selectively in immune cells (Halfon et al., 1998). The official symbol of cystatin F is Cst7, also known as CMAP (cystatin-like metastasis-associated protein) and leukocystatin; in this study we will use CysF for the abbreviation of cystatin F. A major target of CysF is the lysosomal cysteine protease cathepsin C (Hamilton et al., 2008), which is known to regulate the activation of effector granule-associated serine proteases in T cells, natural killer cells, neutrophils and mast cells that are related to immune and inflammatory processes (Adkison et al., 2002; Eyles et al., 2006). The official symbol of cathepsin C is Ctsc, also known as DPP1, DPPI and AI047818, but here we will use CatC as the abbreviation for cathepsin C. In our previous study, CysF was shown to be expressed by activated microglia primarily in the white matter during acute demyelination and active remyelination, but its expression was terminated during the chronic demyelinating phase (at 8 months of age) except in regions where the myelin remained intact. Moreover, in MS, CysF expression is limited to the remyelinating plaques but not found within the chronic lesions, consistent with the pattern in the *Plp*$^{4e/-}$ mouse model of demyelinating disease (Ma et al., 2011).

In this study, we investigated the roles of CatC and CysF in *Plp*$^{4e/-}$ mice. We generated novel transgenic mouse lines in which the levels of CatC or CysF can be manipulated by use of the Flexible Accelerated STOP Tetracycline Operator knockin (FAST) system (Tanaka et al., 2010). We show that the balance between CatC and CysF expression in the brain controls remyelination in chronic demyelinating lesions. These results

should aid in the development of novel and effective treatments for MS and other demyelinating diseases.

Materials and Methods

Ethics statement

All animal procedures were conducted in accordance with the guidelines described by the National Institutes of Health Guide for the Care and Use of Laboratory Animals, and approved by the National Institute for Physiological Sciences Animal Care and Use Committee. The generation of STOP-tetO mice was in accordance with the guidelines set by the animal welfare committee and the ethics committee of Niigata University.

Generation of STOP-tetO knockin mice

The targeting vector containing the 10 kb 3'- homology arm, Neo STOP-tetO cassette, 1.8 kb 5'- homology arm, and diphtheria toxin A subunit (DTA) was designed to insert the Neo STOP-tetO cassette just upstream of the cathepsin C or cystatin F translation initiation site (Tanaka et al., 2010). The C57BL/6N ES cell line RENKA (Mishina and Sakimura, 2007) was used for the recombination. Chimeric mice were mated with C57BL/6N mice, and germline-transmitted offspring were established as CatC STOP-tetO and CysF STOP-tetO heterozygous knockin mice (CatC $^{STOP\text{-}tetO/+}$and CysF$^{STOP\text{-}tetO/+}$, respectively).

Southern blotting

Genomic DNA was digested with *SpeI* or with *PstI* and *EcoRI* for 5'- and 3'-homology arms of CatC STOP-tetO mice, and with *AflII* or with *XbaI* and *EcoRV* for the 5'- or 3'- homology arms of CysF STOP-tetO mice, respectively. The fragments were separated on a 0.8% agarose gel, and blotted onto a nylon membrane. ^{32}P-random-prime-labeled probe (Prime-it II, Stratagene, La Jolla, CA) was hybridized. The probe positions for the 5'- and 3'- homology arms were from -4048 to -3029 or from -3036 to -2077 bases upstream, and from 5373 to

6103 or from 4615 to 5664 bases downstream from the translation initiation site of CatC or CysF, respectively. The probes were located outside of and within the 5'- and 3'-homology arms, respectively. Predicted sizes were: 10 kb and 6.8 kb (*Spe*I digestion) for the 5'-homology arm in the wild type allele and the CatC STOP-tetO allele; and 10 kb (*Pst*I digestion) or 5 kb (*Eco*RI digestion) in the wild type allele and 8 kb (*Pst*I digestion), 5 kb (*Eco*RI digestion) in the CatC STOP-tetO allele for the 3'-homology arm, and 8.5 kb and 5.7 kb (*Afl*II digestion) for the 5'- homology arm in the wild type allele and the CysF STOP-tetO allele; and 11 kb (*Xba*I digestion) and 12 kb (*Eco*RV digestion) in the wild type allele and 7.5 kb (*Xba*I digestion), 12 kb (*Eco*RV digestion) in the CysF STOP-tetO allele for the 3'-homology arm, respectively.

Animals

We used the hemizygous *Plp1* transgenic mouse strain 4e ($Plp^{4e/-}$; C57Bl6/DBA2 mixed background; Kagawa et al., 1994), CysF STOP-tetO mouse ($CysF^{STOP\text{-}tetO/+}$), CatC STOP-tetO mouse ($CatC^{STOP\text{-}tetO/+}$) (both C57BL/6N background) and Iba1-tTA mouse line 75 (initial BDF1 background backcrossed to C57BL/6 background; Tanaka et al., 2012). Genotyping of the $Plp^{4e/-}$ and Iba1-tTA mice was performed as described previously (Kagawa et al., 1994; Tanaka et al., 2012). For CysF STOP-tetO mice, we used CysF 791L: 5'-GCTGCTGTTATGCTTGATCCC-3', CysF 708L: 5'-TCTCAGGGTTCCAAGAGTGTCC-3', CysF 202U: 5'-TTTCTTCACATCAGCATCCC-3' and tetOup: 5'-AGCAGAGCTCGTTTAGTGAACCGT-3' primers. For CatC STOP-tetO mice, CatC205L:5'-AAGGCAAGGACTCAGGGACAGAAA-3', CatC361U: 5'-TTTGGCGTTCCTTGAAAGGCAGAG-3' and tetOup primers. To detect the CysF or CatC WT allele, we used CysF202U and CysF708L (PCR product size: 910 bp), or CatC361U and CatC205L (PCR product size: 566 bp), respectively. To detect the CysF STOP-tetO or CatC

STOP-tetO KI allele, we used tetOup and CysF791L (PCR product size: approximately 930 bp) or CatC205L (PCR product size: approximately 340 bp), respectively.

Preparation of primary cultured microglia and immunocytochemistry

The previously reported method for rat primary microglial cultures (Sawada et al., 1990; Suzumura et al., 1987) was applied to mouse. Microglial cells were harvested from primary mixed glial cell cultures prepared from neonatal CD1 mouse brains (Charles River, Kanagawa, Japan). In brief, after carefully removing the meninges, neonatal brain was dissociated by gentle pipetting. The cell suspension was plated in 75 cm^2 culture flasks (Falcon 3024: Becton-Dickinson Japan, Tokyo, Japan) at a density of five brains per 12 flasks in 10 ml Eagle's minimum essential medium supplemented with 10% fetal bovine serum, 5 mg/ml bovine insulin, and 0.2% glucose. Microglial cells were isolated on days 14-21 on a rotary shaker as previously reported (Suzumura et al., 1987) and cultured in the medium for two days. Two days after microglial separation, immunocytochemistry was performed as described previously (Shimizu et al., 2013). The following primary antibodies were used: rabbit anti-Iba1 polyclonal antibody (1:1000; Wako, Osaka, Japan), rabbit anti-cystatin F polyclonal antibody (1:1000; Gift from Prof. Colin Watts, University of Dundee), mouse anti-cathepsin C polyclonal antibody (1:100; R&D system, Minneapolis, MN).

Cathepsin C activity assay

Fresh brain tissues from $CatC^{STOP\text{-}tetO/+}$ and CatCOE mice were homogenized in 100 μl of lysis buffer (1% Triton-X-100 in PBS) per 10 mg of brain tissue two times for 10 seconds on ice using a potter homogenizer and centrifuged at 10,500 g at 4°C for 15 min. Supernatants were collected and used in the activity assay to measure CatC activity in the transgenic mice. Reaction mixtures containing 50 mM NaAc pH 5.5, 30 mM NaCl, 1 mM DTT, 0.5 mM

EDTA, 10 mM *o*-phenanthroline, 10 μg/ml Pepstatin A and sample were prepared. After pre-incubation of the reaction mixtures for 2 min at room temperature, 100 μM substrate (H-GlyArg-β-naphthylamide in DMSO, BACHEM, Torrance, CA) was added and incubated for 15 min at 37°C. Fluorescence intensity (Excitation 335 nm, Emission 405 nm) was monitored for 15 min at 30 sec intervals to determine the initial rates based on initial velocity (v) using 4-Methoxy-β-naphthylamine as a reference compound.

In Situ hybridization and immunohistochemistry

Mice were perfused intracardially through the left ventricle with 4 % paraformaldehyde (PFA), and brains and spinal cords were dissected out. The tissues were post-fixed with 4 % PFA overnight and cryoprotected with 20 % sucrose-PBS buffer overnight and frozen. Cryosections were prepared at 20 μm thickness with a cryostat and used for in situ hybridization (ISH) and immunohistochemistry (IHC). ISH was performed as described (Ma et al., 2011). The following plasmids containing mouse cDNA were used to generate the ISH probes: *c-fms* (Ma et al., 2011), *cystatin F* (Ma et al., 2011), and *cathepsin C* (nucleotides 193-1324 corresponding to NM_009982.4).

Immunohistochemistry was performed as described (Shimizu et al., 2013). The following primary antibodies were used: rabbit anti-Iba1 polyclonal antibody (1:1000; Wako, Osaka, Japan), rabbit anti-cystatin F polyclonal antibody (1:1000; Gift from Prof. Colin Watts, University of Dundee), mouse anti-cathepsin C polyclonal antibody (1:100; R&D system, Minneapolis, MN), mouse anti-CNPase monoclonal antibody (1:1000; Sigma, St. Louis, MO), goat anti-arginase-1 polyclonal antibody and rat anti-CD16/32 monoclonal antibody (1:200; Santa Cruz, CA, USA). Secondary antibodies were labelled with biotin (Vectastain) or were FITC-conjugated (Invitrogen, Carlsbad, CA). DAB coloring was

performed as described previously (Ma et al., 2011). Images were captured using an Olympus digital camera system (DP70) in combination with a microscope (Olympus BX51).

Image analysis and statistical analyses

The myelin-stained region (area of CNPase labelling) was quantified by measuring the density using the Image J program for densitometric analysis (National Institutes of Health, Bethesda, MD, USA). Data were expressed as the mean ± S.E.M. Significance was assessed by an unpaired two-tailed Student's *t*-test using GraphPad Prism version 5.0b statistics software (GraphPad Software, Inc., La Jolla, CA, USA). *P*-values of less than 0.05 were considered significant.

Electron microscopy

Mice were perfused intracardially through the left ventricle with a fixative containing 2.5 % (v/v) glutaraldehyde and 2.0 % (w/v) PFA in 0.1 M cacodylate buffer (pH 7.4). Brains were dissected and immersed in the same fixative for a couple of days at 4 °C, then 0.5 mm-thick para-sagittal slices were cut with a razor blade and 2 mm x 1.5 mm blocks from the cerebellar lobes were processed for electron microscopy. After osmification in a 1 % (w/v) osmium tetroxide solution for 2 h at 4 °C, the specimens were dehydrated through a graded alcohol series and embedded in Epon 812 (TAAB Laboratories, Aldermaston, UK). Semi-thin sections at 1 μm thickness were collected, stained with 0.5% (w/v) Toluidine blue in 0.1 M PB and imaged with a light microscope (Olympus) equipped with an auto-digitizer to generate "virtual slides" (NanoZoomer-RS, Hamamatsu Photonics). For whole area analysis of the same specimens by EM, ultrathin sections were cut on an ultramicrotome (Ultracut UCT, Leica, Germany) without trimming, collected on platinum-coated glass slides, stained with uranyl acetate and lead citrate and imaged with a scanning electron microscope

equipped with a back-scattered electron beam detector (SU8010, Hitachi, Japan) at 1.5 KV accelerating voltage. From each section, a digitized image with an area of about 200 μm by 300 μm was captured at a resolution of 24.8 nm/pixel.

Results

Spatial and temporal expression pattern differences of cathepsin C and cystatin F between active remyelinating and chronic demyelinated phases

In *Plp*$^{4e/-}$ mice, while spontaneous myelin degeneration starts at 2 months of age, rapid axon remyelination occurs until 6 months of age. After 6 months, the maturation of oligodendrocytes is arrested and remyelination ceases (Ma et al., 2006; Shimizu et al., 2013). We previously found that *CysF* gene expression was greatly reduced at 8 months of age compared to 4 and 6 months in *Plp*$^{4e/-}$ mice (Ma et al., 2007; Ma et al., 2011). It has been reported that a major target of CysF is a cysteine protease, CatC (Hamilton et al., 2008). Thus we examined *CatC* mRNA expression in *Plp*$^{4e/-}$ mice at different time points. At the onset of myelin degeneration in *Plp*$^{4e/-}$ mice at 2 months of age, *CysF* mRNA expression began (Fig. 1A, C), however, *CatC* mRNA was not yet detected (Fig. 1B, D). During the subsequent demyelination/remyelination phase at 4 months of age, the *CysF* expression pattern was similar to that of *CatC* (Fig. 1E-H). At 7 months of age, the expression of both *CysF* and *CatC* was reduced. However, the reduction in *CysF* mRNA expression seemed more rapid than that of *CatC* (Fig. 1I-N); thus, in some regions, *CysF* expression had mostly disappeared (Fig. 1M) while *CatC* expression continued (Fig. 1N). From these results we concluded that *CysF* expression starts earlier than *CatC,* when demyelination is ongoing, but terminates its expression earlier than *CatC* in *Plp*$^{4e/-}$ mice. CysF and CatC were shown to be lysosomal proteins in a cell line of human leukemic monocyte lymphoma, U937, and in hypoxic–ischemic brains (Hamilton et al., 2008; Koike et al., 2013). We attempted to co-stain the same section for both CatC and CysF, which are expressed in lysosomes, but *PLP*$^{4e/-}$ transgenic mice have lipofuscin granules which auto-fluoresce in demyelinating lesions (data not

shown). This strong fluorescence prevented us from detecting proteins in demyelinating brain tissue from $Plp^{4e/-}$ mice by immuno-fluorescence.

Thus, in order to determine if CysF protein colocalizes with CatC protein in microglia, we utilized mouse primary cultured microglia. We found that CysF did colocalize with CatC (Fig. 1O), suggesting that CatC activity can be inhibited by CysF in microglia.

Generation of STOP-tetO knockin mice to manipulate *CatC* and *CysF* gene expression

To study the role of CatC and CysF in demyelinating diseases, we generated transgenic mouse lines in which CatC or CysF expression can be manipulated using the FAST system we established previously (Tanaka et al., 2010). We crossed those mouse strains with $Plp^{4e/-}$ mice to examine the roles of CatC and CysF during the remyelinating/demyelinating stages using the FAST system. The STOP sequence in the FAST system forces termination of transcription (Supplement 1, 2); thus, homozygous mice bearing the STOP-tetO knockin alleles in the absence of the tTA allele ($CatC^{STOP\text{-}tetO/STOP\text{-}tetO}$, $CysF^{STOP\text{-}tetO/STOP\text{-}tetO}$) should behave as knockdown (KD)/knockout (KO) mice because of the STOP sequence. In this study, we refer to $CatC^{STOP\text{-}tetO/STOP\text{-}tetO}$ and $CysF^{STOP\text{-}tetO/STOP\text{-}tetO}$ as CatCKD and CysFKD, respectively.

In adult wild type mice, CatC protein and mRNA were found only in the CA2 region of the hippocampus and choroid plexus (Fig. 2A, B), and were not found in any other regions of the brain. In the CatCKD mouse, *CatC* mRNA and protein were suppressed by the STOP sequence, as expected (Fig 2C, D). CysF was not found in any area of the brain at either postnatal developmental stages or in adults (data not shown, Ma et al., 2011) but *CysF* mRNA and protein were induced during the acute demyelination and active remyelination process in $Plp^{4e/-}$ mice at 4 months of age (Fig. 2E, F, H, I). CysFKD mice on the $Plp^{4e/-}$ background at 4 months of age were devoid of *CysF* mRNA, as expected (Fig. 2G, J).

Generation of Cathepsin C or Cystatin F overexpression in mouse microglia using the FAST system

Since we found that CatC and CysF colocalized within microglia (Fig. 1O), we generated microglia-selective CatC and CysF overexpressing mice as a gain-of-function study. The overexpression of CatC (CatCOE; $CatC^{STOP\text{-}tetO/+}$:: Iba1-tTA) or CysF (CysFOE; $CysF^{STOP\text{-}tetO/+}$:: Iba1-tTA) was achieved by crossing respective STOP-tetO knockin mice with the microglia-selective tTA-expressing line Iba1-tTA.

To confirm the tTA-mediated CysF overexpression, brains from postnatal day 21 (P21) mice were examined. Iba1-tTA mice did not show any CysF expression (Fig. 3A, E), whereas CysFOE mice showed abundant *CysF* mRNA (Fig. 3B) and protein (Fig. 3F) without increasing the number of microglia (Fig. 3C, D). In these mice, all *CysF* mRNA-positive cells were also Iba1-positive ([$CysF^{+}Iba1^{+}$] / [total $Iba1^{+}$] ≃90%; Fig. 3G).

CysF is known to be glycosylated (Ni et al., 1998), and both the monomeric and slowly migrating glycosylated forms were detected (Fig. 3I), consistent with a report by Hamilton et al. (Hamilton et al., 2008). However, the ratio of *CysF* mRNA and Iba1 double-positive cells to the total number of Iba1-positive cells in 11-week-old CysFOE mice ([*CysF*+Iba1+]/[total Iba1+] ≃ 50%; Fig. 3H) was greatly decreased compared to that in P21 mice (Fig. 3G). Thus, either CysF expression driven by the tTA-tetO system was shut down, or the level of *CysF* mRNA derived from this system was below the limit of detection by ISH through an unknown mechanism.

In wild type mice, CatC is expressed mainly in the CA2 region of the hippocampus and choroid plexus (Fig. 2A, B). In CatCOE mice, CatC-overexpressing Iba1-positive cells were observed throughout the entire brain (about 70% of cells were $CatC^{+}Iba1^{+}$; Fig. 4A-C). The enzymatic activity of CatC in the brain of CatCOE mice was examined using a specific

substrate (H-Gly-Arg-β-naphthylamide) and was found to be greatly increased compared to controls, indicating that induced CatC protein has enzymatic activity (Fig. 4D).

From these crosses, we succeeded in obtaining CysFKD, CatCKD and CatCOE mice. Unfortunately, the CysFOE mice generated using this recombination system did not show the gene expression expected to be derived from the tTA-tetO system. Therefore, the use of the CysFOE mice was omitted from this study.

Phenotypic evaluation in mice with *CysF* or *CatC* genetic manipulations

In these mice in which we manipulated the expression of microglial genes, it was necessary to evaluate the differences between WT and CysFKD, CatCKD or CatCOE mice during adult stages. None of these transgenic lines showed any overt phenotypes or clinical symptoms, therefore we examined the specific microglial morphology in these mice. Given that adult mice are needed to evaluate demyelinated lesions, we used two-month-old mice for this experiment. In wild type mice, the microglial morphology, as detected by Iba-1 IHC, showed a normal "resting" shape, i.e. small cell body and numerous very thin and highly branched processes (Fig. 5A). In CatCKD mice, the morphology of the microglia remained in the resting stage, similar to wild type mice (Fig. 5A, B). In contrast, in both the CysFKD (Fig. 5C) and CatCOE mice (Fig. 5D), the "activated" microglia phenotype was found, characterized by shorter and thicker processes with a swollen cell body. Previous studies showed that the *CysF* knockout mice do not show any clinical symptoms or behavioral abnormalities (Mouse genomic informatics, MGI, 2008). However, our results from this histological examination suggested abnormal microglial activation in adult CysFKD mice, and that *CysF* is necessary for the resting microglial phenotype at two months of age, even if the mRNA expression may somehow be below the detection limit by ISH in WT mice.

CysF deprivation enhanced demyelination in *Plp$^{4e/-}$* mice.

In *Plp$^{4e/-}$* mice at 4 months of age, when simultaneous myelin degeneration and regeneration is occurring, both CysF and CatC are expressed in the white matter of demyelinating lesions (Fig. 1E-H and O). To explore the role of CysF during this active remyelinating phase in *Plp$^{4e/-}$* mice, we crossed *Plp$^{4e/-}$* and CysF$^{STOP\text{-}tetO}$ mice to generate CysFKD::*Plp$^{4e/-}$* mice. We stained brain tissues from 4-month-old CysFKD::*Plp$^{4e/-}$* and control (CysF$^{STOP\text{-}tetO/+}$::*Plp$^{4e/-}$*) mice for CNPase and quantified the CNPase-positive area. The CNPase staining from a single cerebellar folium in parasagittal sections is shown in Fig.6 (D), and was measured as described in the Materials and Methods. CysFKD::*Plp$^{4e/-}$* mice showed more severe myelin loss compared to control mice (Fig. 6 A-C). The percentage of the CNPase-stained area in a single cerebellar folium from CysFKD::*Plp$^{4e/-}$* mice was significantly decreased (5.15 ± 0.86%, n = 6) compared to the control group (10.63 ± 0.49%, n = 5; Fig. 6C). We also examined the olfactory tracts and found that 4-month-old CysFKD::*Plp$^{4e/-}$* mice also showed a significant decrease (37.78 ± 1.52%, n =6) compared to the control group (50.05 ± 1.42%, n = 5). These results demonstrated that genetic manipulation to eliminate CysF results in aggravated early phase demyelination in the *Plp$^{4e/-}$* mouse model of chronic demyelination. This suggests that CysF is important for maintaining myelin regeneration.

CatC overexpression also enhanced demyelination in *Plp$^{4e/-}$* mice.

Given that the increase in CatC activity resulting from CysF deprivation exacerbated demyelination (Fig. 1I-N, Fig. 5 A, C, and Fig. 6A-C), the overexpression of the *CatC* gene in *Plp$^{4e/-}$* mice should result in a similar phenotype to CysFKD mice, i.e. enhanced demyelination. Thus, CatCOE::*Plp$^{4e/-}$* mice were analyzed to examine the effect of microglial CatC overexpression on demyelination. CatCOE::*Plp$^{4e/-}$* mice showed more severe myelin

loss at 4 months of age (when we examined the effect of CysFKD on demyelination in CysFKD::*Plp*$^{4e/-}$ mice), and many CatCOE::*Plp*$^{4e/-}$ mice died by 4 months of age (data not shown). Thus, we chose an earlier time point at 2.5 months of age to analyze CatCOE::*Plp*$^{4e/-}$ and *Plp*$^{4e/-}$ mice for the effects of CatCOE on demyelination. We found more severe myelin loss in CatCOE::*Plp*$^{4e/-}$ mice compared to the *Plp*$^{4e/-}$ mice used here as controls (Fig. 7A-B). We quantified the CNPase-stained area in a single cerebellar folium in parasagittal sections, as shown in Fig. 6D. The percentage of the CNPase-stained area in the CatCOE::*Plp*$^{4e/-}$ mice was significantly decreased (5.10 ± 0.36%, n = 8) compared to the control group (7.86 ± 0.64%, n = 4; Fig. 7C). We also examined the olfactory tracts and found that, at 2.5 months of age, CatCOE::*Plp*$^{4e/-}$ mice showed a significant decrease (43.42 ± 3.09%, n =8) compared to control *Plp*$^{4e/-}$ mice (63.65 ± 2.54%, n = 4). Furthermore, we performed electron microscopic (EM) imaging of the cerebellum from CatCOE::*Plp*$^{4e/-}$ and *Plp*$^{4e/-}$ mice (Fig. 7D and E). We observed massive myelin loss in CatCOE::*Plp*$^{4e/-}$ mice at 2.5 months of age, while myelin was maintained in *Plp*$^{4e/-}$ mice of the same age (Fig. 7A and B). This is consistent with the results obtained using the CysFKD mice. These results indicate that the balance between CatC and CysF is very important for maintaining myelin regeneration during the early phase of demyelinating diseases.

CatC knockdown rescued the chronic demyelinating lesions in *Plp*$^{4e/-}$ mice.

Given that CatCOE and CysFKD in *Plp*$^{4e/-}$ mice showed exaggerated demyelination, we sought to reverse the balance of CatC/CysF expression using CatCKD mice. To examine the impact of CatC knockdown on demyelination, we used CatCKD::*Plp*$^{4e/-}$ mice and CatC$^{STOP\text{-}tetO/+}$::*Plp*$^{4e/-}$ mice as controls, and analyzed the phenotypes of these mice at 4, 6 and 8 months of age. There were no significant differences in the CNPase-positive areas between CatCKD::*Plp*$^{4e/-}$ and CatC$^{STOP\text{-}tetO/+}$::*Plp*$^{4e/-}$ mice at 4 months of age when active

remyelination is ongoing (data not shown). CatC$^{STOP\text{-}tetO/+}$::*Plp*$^{4e/-}$ mice gradually lost myelin in this region at 6 months of age (Fig. 8A) and clearly showed severe myelin loss at 8 months of age (Fig. 8C). However, CatCKD::*Plp*$^{4e/-}$ mice had substantially more remaining myelin compared to CatC$^{STOP\text{-}tetO/+}$::*Plp*$^{4e/-}$ mice (Fig. 8A-D). We quantified the CNPase-stained area in a single cerebellar folium from parasagittal sections as shown in Fig. 6 and 7. The percentage of the CNPase-stained areas in CatCKD::*Plp*$^{4e/-}$ mice (14.11 ± 1.25%, n = 9) was significantly higher than in CatC$^{STOP\text{-}tetO/+}$::*Plp*$^{4e/-}$ mice (7.90 ± 2.97%, n = 3) at 8 months of age (Fig. 8F), while no significant differences were found at 6 months of age (Fig. 8E; n=3 mice each per group). We also examined the olfactory tracts and found that CatCKD::*Plp*$^{4e/-}$ mice at 8 months of age showed a significantly higher percentage of stained area (47.62 ± 5.27%, n= 9) compared to control CatC$^{STOP\text{-}tetO/+}$::*Plp*$^{4e/-}$ mice (21.80 ± 1.37%, n=3). To confirm this result, we performed EM imaging of these mice. More myelinated axons were observed in CatCKD::*Plp*$^{4e/-}$ mice (Fig. 8 H) compared to controls (Fig. 8 G). We also quantified the number of myelinated axons for each diameter range. We found that CatCKD::*Plp*$^{4e/-}$ mice at 8 months of age had an increased number of myelinated axons with larger diameters (myelinated axon diameter between 1 and 3.5 μm) compared to WT mice of the same age (Fig. 9A). We also found that CatCKD::*Plp*$^{4e/-}$ mice had a higher average g-ratio compared to WT mice, indicating that CatCKD::*Plp*$^{4e/-}$ mice had thinner myelin sheaths and that CatCKD promoted remyelination in *Plp*$^{4e/-}$ mice (Fig. 9B). These results show that the balance between CatC and CysF is an important factor controlling the myelin regeneration process even during late stages of chronic demyelinating diseases. During the chronic demyelinating phase in which CatC expression dominates CysF expression, CatC deprivation can rescue *Plp*$^{4e/-}$ mice from severe demyelination.

Discussion

In chronic MS lesions, the remyelination process is impaired resulting in demyelinated lesions (Chang et al., 2002; Kuhlmann et al., 2008; Noseworthy, 1999). The most crucial question is what factors govern the oligodendrocyte precursor recruitment and oligodendrocyte differentiation phases of remyelination, and whether misregulation of any of these factors can account for remyelination failure. Previous studies have identified several pathways with the potential to have therapeutic efficacy (Fancy et al., 2010). We had previously reported that microglia express CysF only during the active remyelinating stage (at 4-6 months) and that downregulation of CysF expression indicates the cessation of remyelination in demyelinating regions (Ma et al., 2011). CysF is a specific inhibitor of CatC, and CatC mediates the generation of pro-inflammatory cytokines such as tumor necrosis factor-α (TNF-α) which is highly toxic to oligodendrocytes, and interleukin 1-β (IL-1β) a remyelination promoting factor (Adkison et al., 2002; Hamilton et al., 2008; Mason et al. 2001, McLaurin et al., 1995; Ye and D'Ercole, 1999). Thus, CysF could be one of the factors specifically influencing differentiation and/or survival. Here, we studied the roles of CatC and CysF in mouse models in which it was possible to manipulate the expression of CatC and CysF.

This study demonstrated that the CysF/CatC system is one possible mechanism that may inhibit myelin regeneration. We found activated microglia in adult CysFKD and CatCOE mice. However, CatC knockdown mice did not show any overt phenotypes. In CatCOE and CysFKD mice, the increase in CatC and deprivation of its inhibitor CysF might increase CatC activity in microglia causing the microglia themselves to become activated. Maintenance of the brain environment is very important for the recovery process from injury, diseases or infection; this includes the phagocytosis of debris and secretion of growth signals, cytokines and other factors. Microglial cells monitor the wellbeing of their environment and

are able to respond to signs of homeostatic disturbance with a program of supportive and protective activity, to safeguard innate defense mechanisms, or to assist in specific immune responses (Hanisch, 2002; Kotter et al, 2006; Lampron et al., 2015; Stollg and Jander, 1999). Activated microglia have been found to persist in chronic demyelinating lesions (Tanuma et al., 2006; Taupin et al., 1997). It seems that changes in the normal levels of CatC or CysF beyond physiological levels cause a disturbance in the brain homeostasis and the activation of microglia. It is possible that CatC and CysF could send crucial signals that alert the CNS to prepare microglia which can respond to any type of CNS disturbance.

In $Plp^{4e/-}$ mice, *CysF* and *CatC* had similar expression patterns during the active remyelinating phase at 4 months of age, shown in Fig. 1E-H. However, CysF was found to be expressed earlier than CatC during active demyelination and remyelination (Fig.1 A-D) when it dominated CatC expression prior to the emergence of chronic lesions (Fig. 1A-H). During this phase, the myelin regeneration process is very important for maintaining the myelin sheath; this is similar to the early phase of MS which shows relapse-remission symptoms (Niehaus et al., 2000). At 2 months of age, $Plp^{4e/-}$ mice show neither paralysis nor muscular dystrophy defects, but do show signs of nerve conduction disturbance (Tanaka et al., 2006) and tonic seizures similar to the early symptoms of MS (Kelley and Rodriguez, 2009). CysF induction in microglia is dependent on the phagocytosis of compact myelin membranes (Ma et al., 2011), thus CysF might have a role in supporting the myelin regeneration process. Here we showed that *CysF* knockdown in $Plp^{4e/-}$ mice resulted in exaggerated demyelination at earlier phases of demyelination. CysF inhibits CatC protease activity and disrupts downstream signals that can cause disturbance in the myelin regeneration process. (Hamilton et al., 2008; Irmler et al., 1995; Pham and Ley, 1999). The balance between CatC and CysF expression also seems to play a critical role in myelin regeneration during the early phase of chronic demyelinating diseases. This conclusion was confirmed by CatC overexpression in

microglia showing severe demyelination at a very early phase of chronic demyelination. In the early phase of chronic demyelinating disease, CysF should play a dominant role in supporting myelin regeneration by interfering with CatC function. In this study, we showed only a lobe of the cerebellum and olfactory tracts for statistical analysis, although *Plp*$^{4e/-}$ mice undergo demyelination throughout the entire CNS. While demyelination does not typically proceed uniformly and shows some regional variation, even among individuals, the demyelination we observed in the cerebellum and olfactory tracts was relatively constant. Therefore, we chose these regions for our statistical analysis.

During the late phase of chronic demyelinating disease, CatC was found to dominate CysF and full activation of microglia is expected. This could cause impaired myelin regeneration and the appearance of naked axons in the *Plp*$^{4e/-}$ mice (Kagawa et al., 1994). We found that CatC knockdown resulted in more intact myelin in the late phase of chronic demyelination. This provides strong evidence that CatC is one of the key factors that induces demyelination. The conclusions drawn from this study demonstrated that the balance between CatC and CysF expression plays an important role in chronic demyelinating disease.

Acknowledgments

This work was supported by Grants-in-Aid for Scientific Research on Innovative Areas: “Foundation of Synapse and Neurocircuit Pathology (23110521)”, Japan Society for the Promotion of Science (JSPS), “Glial Assembly: a new regulatory machinery of brain function and disorders (25117001)” and “Thailand Research Fund under the Royal Golden Jubilee-Ph.D. Scholarship and Mahidol University” to WW and BC. The activity assays were performed with help from Akio Suzumura and Tetsuya Mizuno in the Department of Neuroimmunology, Research Institute of Environmental Medicine, Nagoya University, Japan; Yasuo Uchiyama and Masato Koike in the School of Medicine, Juntendo University, Japan; and Masahiro Shibata in Niigata University, Japan. The southern blotting was performed with help from Maya Yamazaki (current affiliation: Niccole lab at the University of California San Francisco, USA). Electron microscopy analysis was performed with help from Katsutoshi Ogasawara and other staff at the Center for Electron Microscopy and Bio-Imaging Research, Iwate Medical University. The anti-cystatin F antibody was generously gifted from Colin Watts (Dundee University). This work was also supported by JSPS KAKENHI (25650181 and 25245069) to KT, a Grant-in-Aid for Strategic Medical Science Research for private university (No. S1491001, 2014-2018) from MEXT to YS.

References

Adkison AM, Raptis SZ, Kelley DG, Pham CT. 2002. Dipeptidyl peptidase I activates neutrophil-derived serine proteases and regulates the development of acute experimental arthritis. J Clin Invest 109:363-371.

Arnoux I, and Audinat E. 2015. Fractalkine signaling and microglia functions in the developing brain. Neural Plast 2015:689404.

Back SA, Tuohy TM, Chen H, Wallingford N, Craig A, Struve J, Luo NL, Banine F, Lui Y, Chang A, Trapp BD, Bebo BF Jr., Rao MS, Sherman LS. 2005. Hyaluronan accumulates in demyelinated lesions and inhibits oligodendrocyte progenitor maturation. Nat Med 11:966-972.

Boven LA, Van Meurs M, Van Zwam M, Wierenga-Wolf A, Hintzen RQ, Boot RG, Aerts JM, Amor S, Nieuwenhuis EE, Laman JD. 2006. Myelinladen macrophages are anti-inflammatory, consistent with foam cells in multiple sclerosis. Brain 129:517-526.

Chang A, Nishiyama A, Peterson J, Prineas J, Trapp BD. 2000. NG2-positive oligodendrocyte progenitor cells in adult human brain and multiple sclerosis lesions. J Neurosci 20:6404-6412.

Chang A, Tourtellotte WW, Rudick R, Trapp BD. 2002. Premyelinating oligodendrocytes in chronic lesions of multiple sclerosis. N Engl J Med 346:165-73.

Charles P, Reynolds R, Seilhean D, Rougon G, Aigrot MS, Niezgoda A, Zalc B, Lubetzki C. 2002. Re-expression of PSA-NCAM by demyelinated axons: an inhibitor of remyelination in multiple sclerosis? Brain. 125:1972-9.

David S, and Kroner A. 2011. Repertoire of microglial and macrophage responses after spinal cord injury. Nat Rev Neurosci 12:388-399.

Eyles JL, Roberts AW, Metcalf D, Wicks IP. 2006. Granulocyte colony-stimulating factor and neutrophils--forgotten mediators of inflammatory disease. Nat Clin Pract Rheumatol 2:500-510.

Fancy SP, Kotter MR, Harrington EP, Huang JK, Zhao C, Rowitch DH, Franklin RJ. 2010. Overcoming remyelination failure in multiple sclerosis and other myelin disorders. Exp Neurol 225:18-23.

Girolamo F, Ferrara G, Strippoli M, Rizzi M, Errede M, Trojano M, Perris R, Roncali L, Svelto M, Mennini T, Virgintino D. 2011. Cerebral cortex demyelination and oligodendrocyte precursor response to experimental autoimmune encephalomyelitis. Neurobiol Dis 43:678-689.

Halfon S, Ford J, Foster J, Dowling L, Lucian L, Sterling M, Xu Y, Weiss M, Ikeda M, Liggett D, Helms A, Caux C, Lebecque S, Hannum C, Menon S, McClanahan T, Gorman D, Zurawski G. 1998. Leukocystatin, a new class II cystatin expressed selectively by hematopoietic cells. J Biol Chem 273:16400-16408.

Hamilton G, Colbert JD, Schuettelkopf AW, Watts C. 2008. Cystatin F is a cathepsin C-directed protease inhibitor regulated by proteolysis. EMBO J 27:499-508.

Hanisch UK. 2002. Microglia as a source and target of cytokines. Glia 40:140-155.

Heppner FL, Greter M, Marino D, Falsig J, Raivich G, Hövelmeyer N, Waisman A, Rülicke T, Prinz M, Priller J, Becher B, Aguzzi A. 2005. Experimental autoimmune encephalomyelitis repressed by microglial paralysis. Nat Med 11:146-152.

Irmler M, Hertig S, MacDonald HR, Sadoul R, Becherer JD, Proudfoot A, Solari R, Tschopp J. 1995. Granzyme A is an interleukin 1 beta-converting enzyme. J Exp Med 181:1917-1922.

Kagawa T, Ikenaka K, Inoue Y, Kuriyama S, Tsujii T, Nakao J, Nakajima K, Aruga J, Okano H, Mikoshiba K. 1994. Glial cell degeneration and hypomyelination caused by overexpression of myelin proteolipid protein gene. Neuron 13:427-442.

Kelley BJ and Rodriguez M. 2009. Seizures in Patients with Multiple Sclerosis: Epidemiology, Pathophysiology and Management. CNS Drugs 23:805-815.

Koike M, Shibata M, Ezaki J, Peters C, Saftig P, Kominami E, Uchiyama Y. 2013. Differences in expression patterns of cathepsin C/dipeptidyl peptidase I in normal, pathological and aged mouse central nervous system. Eur J Neurosci 37:816-830.

Kotter MR, Li WW, Zhao C, Franklin RJ. 2006. Myelin impairs CNS remyelination by inhibiting oligodendrocyte precursor cell differentiation. J Neurosci 26:328–332.

Kreutzberg GW. 1996. Microglia: a sensor for pathological events in the CNS. Trends Neurosci 19:312–318.

Kuhlmann T, Miron V, Cui Q, Wegner C, Antel J, Brück W. 2008. Differentiation block of oligodendroglial progenitor cells as a cause for remyelination failure in chronic multiple sclerosis. Brain 131:1749-1758.

Lampron A, Larochelle A, Laflamme N, Préfontaine P, Plante MM, Sánchez MG, Yong VW, Stys PK, Tremblay MÈ, Rivest S. 2015. Inefficient clearance of myelin debris by microglia impairs remyelinating processes. J Exp Med 212:481-495.

Ma J, Matsumoto M, Tanaka KF, Takebayashi H, Ikenaka K. 2006. An animal model for late onset chronic demyelination disease caused by failed terminal differentiation of oligodendrocytes. Neuron Glia Biol 2:81-91.

Ma J, Tanaka KF, Yamada G, Ikenaka K. 2007. Induced expression of cathepsins and cystatin C in a murine model of demyelination. Neurochem Res 32:311-320.

Ma J, Tanaka KF, Shimizu T, Bernard CC, Kakita A, Takahashi H, Pfeiffer SE, Ikenaka K. 2011. Microglial cystatin F expression is a sensitive indicator for ongoing demyelination with concurrent remyelination. J Neurosci Res 89:639-649.

Mason JL, Suzuki K, Chaplin DD, Matsushima GK. 2001. Interleukin-1β promotes repair of the CNS. J Neurosci 21:7046-7052.

McLaurin J, D'Souza S, Steward J, Blain M, Beaudet A, Nalbantoglu J, Antel JP. 1995. Effect of tumor necrosis factor a and b on human oligodendrocytes and neurons in culture. Int J Dev Neurosci 13:369–381.

Martinez FO, Gordon S, Locati M, Mantovani A. 2006. Transcriptional profiling of the human monocyte-to-macrophage differentiation and polarization: new molecules and patterns of gene expression. J Immunol 177:7303-7311.

Mishina M and Sakimura K. 2007. Conditional gene targeting on the pure C57BL/6 genetic background. Neurosci Res 58:105-112.

Miron VE, Boyd A, Zhao JW, Yuen TJ, Ruckh JM, Shadrach JL, van Wijngaarden P, Wagers AJ, Williams A, Franklin RJ, ffrench-Constant C. 2013. M2 microglia/macrophages drive oligodendrocyte differentiation during CNS remyelination. Nat Neurosci 16:1211-1218.

Mouse genome informatics (MGI). 2008. MGI Ref ID: MGI:1298217. http://www.informatics.jax.org/marker/MGI:1298217. Updated 11/10/2015. Accessed 22, November, 2015.

Ni J, Fernandez MA, Danielsson L, Chillakuru RA, Zhang J, Grubb A, Su J, Gentz R, Abrahamson M. 1998. Cystatin F is a glycosylated human low molecular weight cysteine proteinase inhibitor. J Biol Chem 273:24797–24804.

Niehaus A, Shi J, Grzenkowski M, Diers-Fenger M, Archelos J, Hartung HP, Toyka K, Brück W, Trotter J. 2000. Patients with active relapsing-remitting multiple sclerosis synthesize antibodies recognizing oligodendrocyte progenitor cell surface protein: implications for remyelination. Ann Neurol 48:362-371.

Noseworthy JH. 1999. Progress in determining the causes and treatment of multiple sclerosis. Nature 399:A40-A47.

Pham CT and Ley TJ. 1999. Dipeptidyl peptidase I is required for the processing and activation of granzymes A and B in vivo. Proc Natl Acad Sci USA 96:8627-8632.

Ransohoff RM and Perry VH. 2009. Microglial Physiology: Unique Stimuli, Specialized Responses. Annu Rev Immunol 27:119-145.

Ransohoff RM. 2016. A polarizing question: do M1 and M2 microglia exist? Nat Neurosci 19:987-991.

Sawada M, Suzumura A, Yamamoto H, Marunouchi T. 1990. Activation and proliferation of the isolated microglia by colony stimulating factor-1 and possible involvement of protein kinase C. Brain Res 509:119-124.

Schafer DP, Lehrman EK, Kautzman AG, Koyama R, Mardinly AR, Yamasaki R, Ransohoff RM, Greenberg ME, Barres BA, Stevens B. 2012. Microglia sculpt postnatal neural circuits in an activity and complement-dependent manner. Neuron 74:691-705.

Shemer A, Erny D, Jung S, Prinz M. 2015. Microglia plasticity during health and disease: An immunological perspective. Trends Immunol 36:614-624.

Shimizu T, Tanaka KF, Takebayashi H, Higashi M, Wisesmith W, Ono K, Hitoshi S, Ikenaka K. 2013. Olig2-lineage cells preferentially differentiate into oligodendrocytes but their processes degenerate at the chronic demyelinating stage of proteolipid protein-overexpressing mouse. J Neurosci Res 91:178–186.

Stollg G and Jander S. 1999. The role of microglia and macrophages in the pathophysiology of the CNS. Prog Neurobiol 58:233-247.

Suzumura A, Mezitis SG, Gonatas NK, Silberberg DH. 1987. MHC antigen expression on bulk isolated macrophage-microglia from newborn mouse brain: induction of Ia antigen expression by gamma-interferon. J Neuroimmunol 15:263-278.

Tanaka H, Ikenaka K, Isa T. 2006. Electrophysiological abnormality precedes apparent histological demyelination in the central nervous system of mice over-expressing proteolipid protein. J Neurosci Res 84: 1206-1216.

Tanaka KF, Ahmari SE, Leonardo ED, Richardson-Jones JW, Budreck EC, Scheiffele P, Sugio S, Inamura N, Ikenaka K, Hen R. 2010. Flexible accelerated STOP tetracycline operator-knockin (FAST): a versatile and efficient new gene modulating system. Biol Psychiatry 67:770–773.

Tanaka KF, Matsui K, Sasaki T, Sano H, Sugio S, Fan K, Hen R, Nakai J, Yanagawa Y, Hasuwa H, Okabe M, Deisseroth K, Ikenaka K, Yamanaka A. 2012. Expanding the repertoire of optogenetically targeted cells with an enhanced gene expression system. Cell Rep 2:397–406.

Tanuma N, Sakuma H, Sasaki A, Matsumoto Y. 2006. Chemokine expression by astrocytes plays a role in microglia/macrophage activation and subsequent neurodegeneration in secondary progressive multiple sclerosis. Acta Neuropathol 112:195-204.

Taupin V, Renno T, Bourbonniere L, Peterson AC, Rodriguez M, Owens T. 1997. Increased severity of experimental autoimmune encephalomyelitis, chronic macrophage/microglial reactivity, and demyelination in transgenic mice producing tumour necrosis factor-alpha in the central nervous system. Eur J Immunol 27:905-913.

Trebst C, König F, Ransohoff RM, Brück W, Stangel M. 2008. CCR5 expression on macrophages/microglia is associated with early remyelination in multiple sclerosis lesions. Multiple Sclerosis 14:728-733.

Van Rossum D, Hilbert S, Strassenburg S, Hanisch UK, Brück W. 2008. Myelin-phagocytosing macrophages in isolated sciatic and optic nerves reveal a unique reactive phenotype. Glia 56:271-283.

Ye P and D'Ercole AJ. 1999. Insulin-like growth factor I protects oligodendrocytes from tumor necrosis factor-alpha-induced injury. Endocrinology 140:3063–3072.

Zhang SC, Goetz BD, Duncan ID. 2003. Suppression of activated microglia promotes survival and function of transplanted oligodendroglial progenitors. Glia 41:191-198.

Legends

Figure 1. The expression patterns of *cystatin F* and *cathepsin C* are similar during the active remyelinating phase but not in chronic lesions.

In situ hybridization for *cystatin F* (A, C, E, G, I, K, M) and *cathepsin C* (B, D, F, H, J, L, N) was performed on brain tissues from $Plp^{4e/-}$ mice at 2 (A-D), 4 (E-H) and 7 (I-N) months of age. (A), (B), (E), (F), (I) and (J) are magnified images of the areas outlined in black from (C), (D), (G), (H), (K) and (L), respectively. (M) and (N) are magnified images of the areas outlined in red in (I) and (J), respectively. Immunocytochemistry demonstrated that CatC (shown in red) and CysF (shown in green) were co-localized in primary cultured microglial cells (O). Scale bars: A, 200 μm; C, 600 μm; N, 100 μm; O, 20 μm.

Figure 2. Successful knockdown of Cathepsin C and Cystatin F in homozygous STOP-tetO mice.

Adult wild type and CatCKD mice were analyzed for *CatC* mRNA (A, C) and CatC protein expression (B, D). Four-month-old $Plp^{4e/-}$ mice were analyzed for *CysF* mRNA (E, H) and CysF protein expression (F, I). Four-month-old CysFKD::$Plp^{4e/-}$ mice were analyzed for *CysF* mRNA expression (G, J). H, I and J are magnified images of the corpus callosum region in E, F and G, respectively. Scale bars: 100 μm for A, C, E, G; 50 μm for B, D, F, H, I, J.

Figure 3. Successful overexpression of Cystatin F in Iba1-positive microglia.

In situ hybridization for *CysF* and *c-fms* mRNA, and immunohistochemistry for CysF were performed on spinal cord sections from Iba1-tTA (A, C, E) and CysFOE mice (B, D, F). The inset in (F) is a magnified image of the area outlined in black and indicated by a red arrowhead. Double staining of *CysF* mRNA by *in situ* hybridization and Iba1 by

immunohistochemistry was performed on thoracic spinal cords from CysFOE mice at postnatal day 21 (P21) (G) and at 11 weeks (H). The inset in (G) is a magnified image of the cell outlined in black. Brain lysates from wild type and CysFOE mice were used for cystatin F immunoblotting (I). The arrow indicates monomers of cystatin F and the asterisk indicates the glycosylated slow migrating forms. Scale bars: D, 500 μm; F, 50 μm; H, 200 μm.

Figure 4. Successful overexpression of Cathepsin C in Iba1-positive microglia.

(A-C) CatC and Iba1 are shown in red and green, respectively, in the brain of a CysFOE ($CatC^{STOP\text{-}tetO/+}$::Iba1-tTA) mouse. CatCOE and $CatC^{STOP\text{-}tetO/+}$ mice were analyzed for CatC activity using a specific substrate for cathepsin C (D). The control wells contained buffer and protease substrates only. The florescence signal was measured from time 0 when brain lysate supernatants from CatCOE and $CatC^{STOP\text{-}tetO/+}$ mice were added. Scale bars: A-C, 20 μm.

Figure 5. Morphological analysis of microglia in *CatC* and *CysF* genetically manipulated mice.

Wild type (A), CatCKD (B), CysFKD (C) and CatCOE (D) mice at two months of age were analyzed for microglial morphology in the cerebellum. Parasagittal brain cryosections were used for Iba1 immunohistochemistry to visualize microglial morphology. Scale bar in D, 20 μm.

Figure 6. CysF knockdown worsened the demyelination in $Plp^{4e/-}$ mice.

$CysF^{STOP\text{-}tetO/+}$::$Plp^{4e/-}$ (A) and CysFKD::$Plp^{4e/-}$ (B) mice at 4 months of age were analyzed for myelin loss in the brain by staining for CNPase. $CysF^{STOP\text{-}tetO/+}$::$Plp^{4e/-}$ was used as the control. (C) The percentage of the myelin stained area was quantified by densitometry analysis and the differences between the groups are represented in the graph: $CysF^{STOP\text{-}}$

$^{tetO/+}$::*Plp*$^{4e/-}$ (10.63 ± 0.49%, n=5), CysFKD::*Plp*$^{4e/-}$ (5.15 ± 0.86%, n=6); **p* < 0.05 compared to the control group. (D) Schematic of mouse parasagittal sections. The region indicated by the black dashed line represents the area that was quantified. Scale bars: A and B, 50 μm.

Figure 7. CatC overexpression induced earlier demyelination in *Plp*$^{4e/-}$ mice.

Two-month-old *Plp*$^{4e/-}$ (A) and CatCOE::*Plp*$^{4e/-}$ (B) transgenic mice were assayed for myelin in the brain. The percentage of the CNPase-stained area was quantified by densitometry analysis and differences between the groups are represented in the graph (C): *Plp*$^{4e/-}$ (7.86 ± 0.64%, n=4), CatCOE::*Plp*$^{4e/-}$ (5.10 ± 0.36%, n=8). (D, E) Electron microscopic images of the cerebellar lobe region shown in Fig. 6D from *Plp*$^{4e/-}$ (D) and CatCOE::*Plp*$^{4e/-}$ (E) mice at 2.5 months of age (**p* < 0.05 compared to the control group). Scale bars: A-B, 50 μm; D-E, 10 μm.

Figure 8. CatC knockdown reduced demyelination in *Plp*$^{4e/-}$ mice.

CatC$^{STOP\text{-}tetO/+}$::*Plp*$^{4e/-}$ (A and C) and CatCKD::*Plp*$^{4e/-}$ (B and D) mice were analyzed for the amount of myelin in the brain at 6 and 8 months of age. CatC$^{STOPtetO/+}$::*Plp*$^{4e/-}$ mice were used as controls. The percentage of the myelin stained area was quantified by densitometry analysis and the differences between the groups are represented in the graphs (E and F): CatC$^{STOP\text{-}tetO/+}$::*Plp*$^{4e/-}$ (7.90 ± 2.97%, n=3), CatCKD::*Plp*$^{4e/-}$ (14.11 ± 1.25%, n=9). (G, H) Electron microscopic images of the cerebellar lobe region shown in Fig. 6D from CatC$^{STOP\text{-}tetO/+}$::*Plp*$^{4e/-}$ and CatCKD::*Plp*$^{4e/-}$ mice at 8 months of age (**p* < 0.05 compared to the control group). Scale bars: A-D, 200 μm; G-H, 10 μm.

Figure. 9 Cathepsin C knockdown promoted remyelination in *Plp*$^{4e/-}$ mice.

(A) Distribution of myelinated axon diameters measured at the cerebellar lobe region shown in Fig. 6D from WT and CatCKD::*Plp*$^{4e/-}$ mice at 8 months of age. The vertical axis indicates the number of myelinated axons and the horizontal axis indicates the myelinated axon diameter range. (B) Axon diameter and g-ratio distribution measured at the cerebellar lobe from WT and CatCKD::*Plp*$^{4e/-}$ mice at 8 months of age. The vertical axis indicates axon diameter and the horizontal axis indicates the g-ratio.

Supplementary 1. Construction of CysF STOP-tetO mice and Southern blotting.

(A) The upper figure shows a schematic of the wild type genome, the targeting vector and CysF STOP-tetO allele structures, and the *Afl*II restriction sites; the 5' probe position is indicated by a black bar. Black arrows represent primer positions. Open triangles represent loxP sites. Filled triangles represent FRT sites. Neo is the PGK-EM7-NEO minigene. STOP is the cassette containing elements designed to terminate both transcription and translation. ATG represents the translation initiation site. tetO is the cassette containing the tetracycline operon site and CMV minimal promoter. The lower figure shows the Southern blotting results from genomic DNA of wild type, heterozygote and homozygote CysF STOP-tetO mice. (B) The upper figure shows a schematic of the wild type, targeting vector and CysF STOP-tetO allele structures, as well as the 3' probe position, and *Xba*I and *Eco*RV restriction sites. The lower figure shows the Southern blotting results from genomic DNA of wild type, heterozygote and homozygote CysF STOP-tetO mice.

Supplementary 2. Construction of CatC STOP-tetO mice and Southern blotting.

(A) The upper figure shows a schematic of the wild type genome, the targeting vector and CatC STOP-tetO allele structures, as well as the 5' probe position and *Spe*I restriction sites. The symbols are the same as in Supplementary 1. The lower figure shows the Southern

blotting results from genomic DNA of wild type, heterozygote and homozygote CatC STOP-tetO mice. (B) The upper figure shows a schematic of the wild type genome, the targeting vector and CatC STOP-tetO allele structures, as well as the 3' probe position, and *Pst*I and *Eco*RI restriction sites. The lower figure shows the Southern blotting results from genomic DNA of wild type, heterozygote and homozygote CatC STOP-tetO mice.

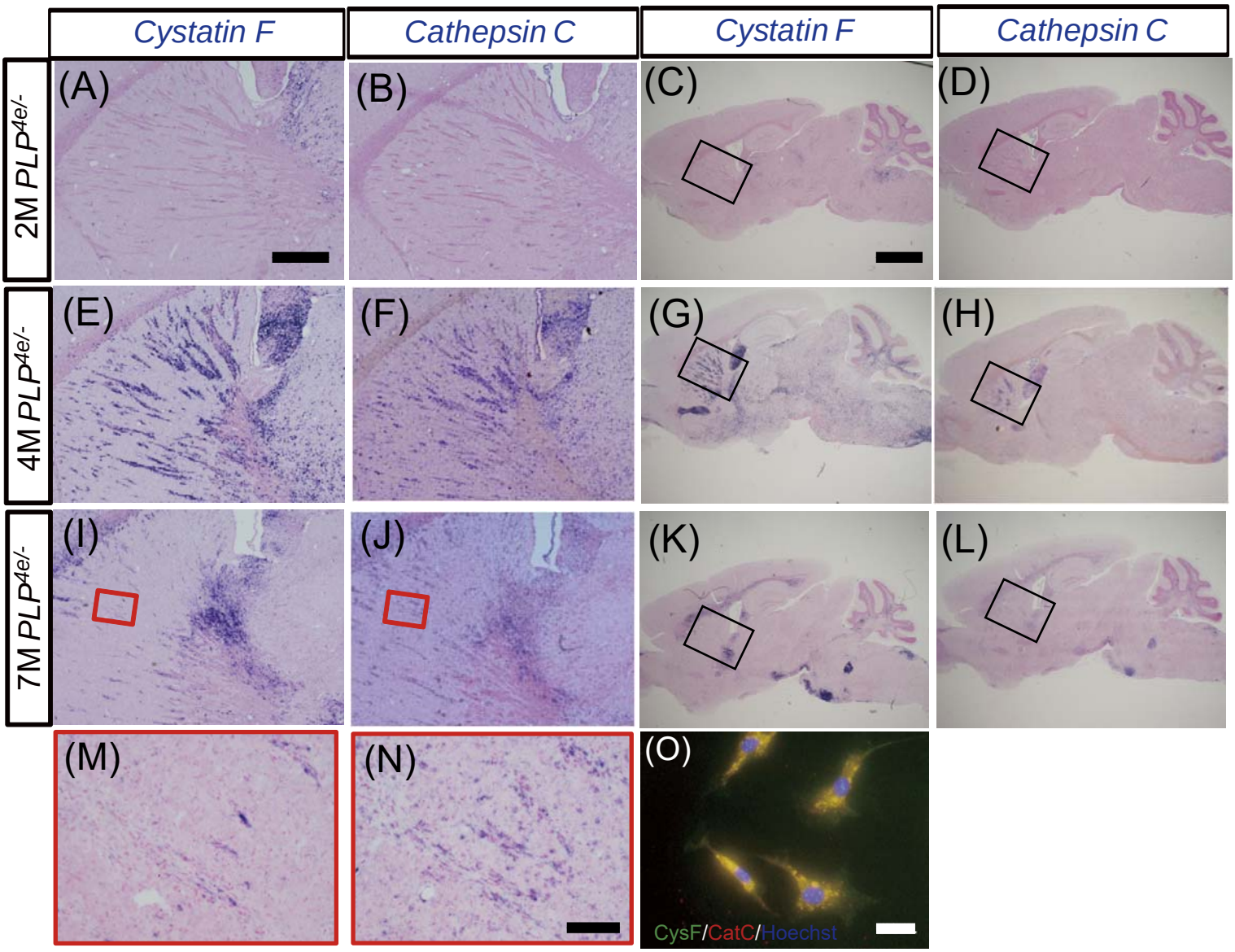
Cystatin F
Cathepsin C
Cystatin F
Cathepsin C
2M PLP4e/-
4M PLP4e/-
7M PLP4e/-
(A)
(B)
(C)
(D)
(E)
(F)
(G)
(H)
(I)
(J)
(K)
(L)
(M)
(N)
(O)
CysF/CatC/Hoechst

Figure 1

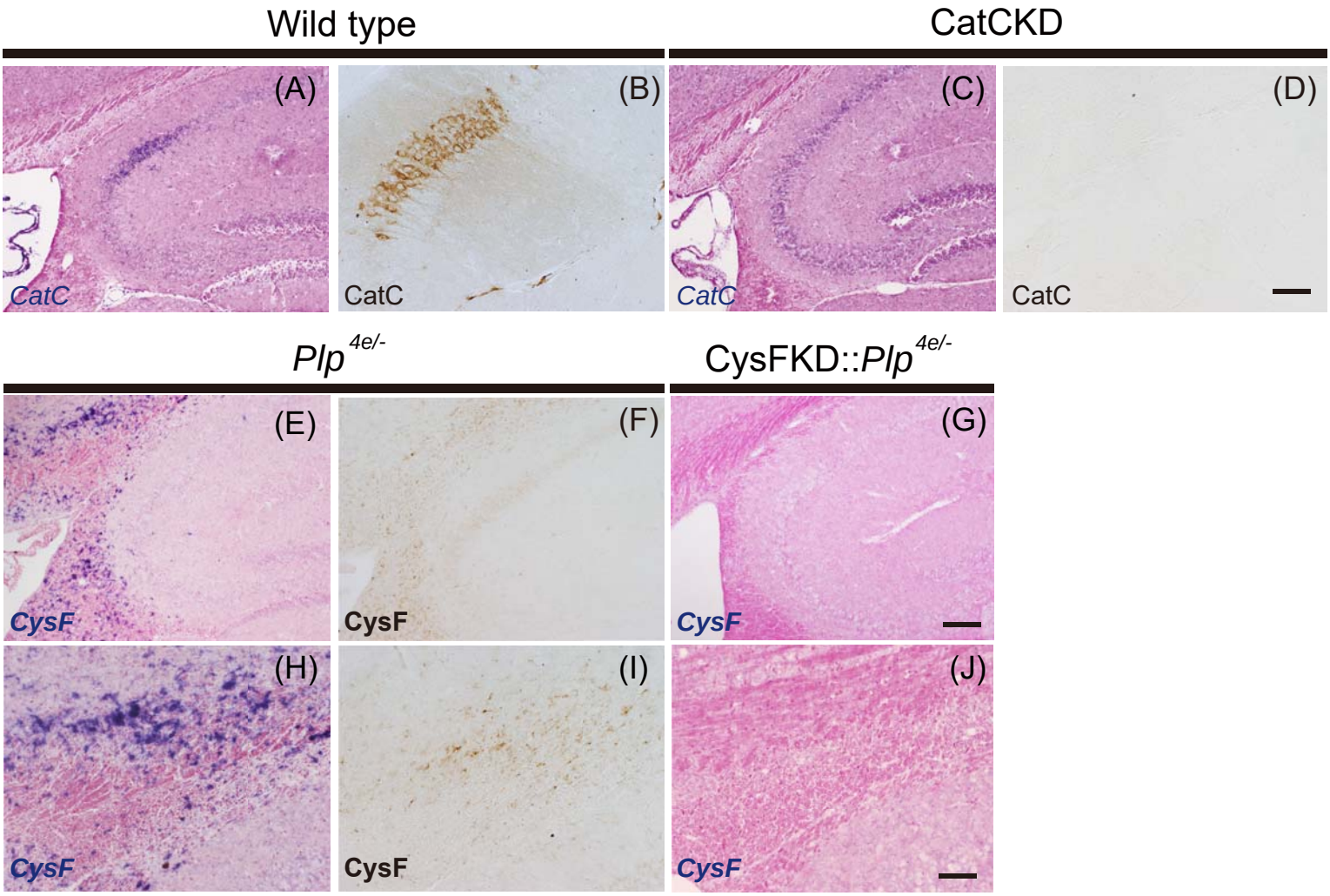
Wild type
CatCKD
(A)
(B)
(C)
(D)
CatC
CatC
CatC
CatC
Plp4e/-
CysFKD::Plp4e/-
(E)
(F)
(G)
(H)
(I)
(J)
CysF
CysF
CysF
CysF
CysF
CysF

Figure 2

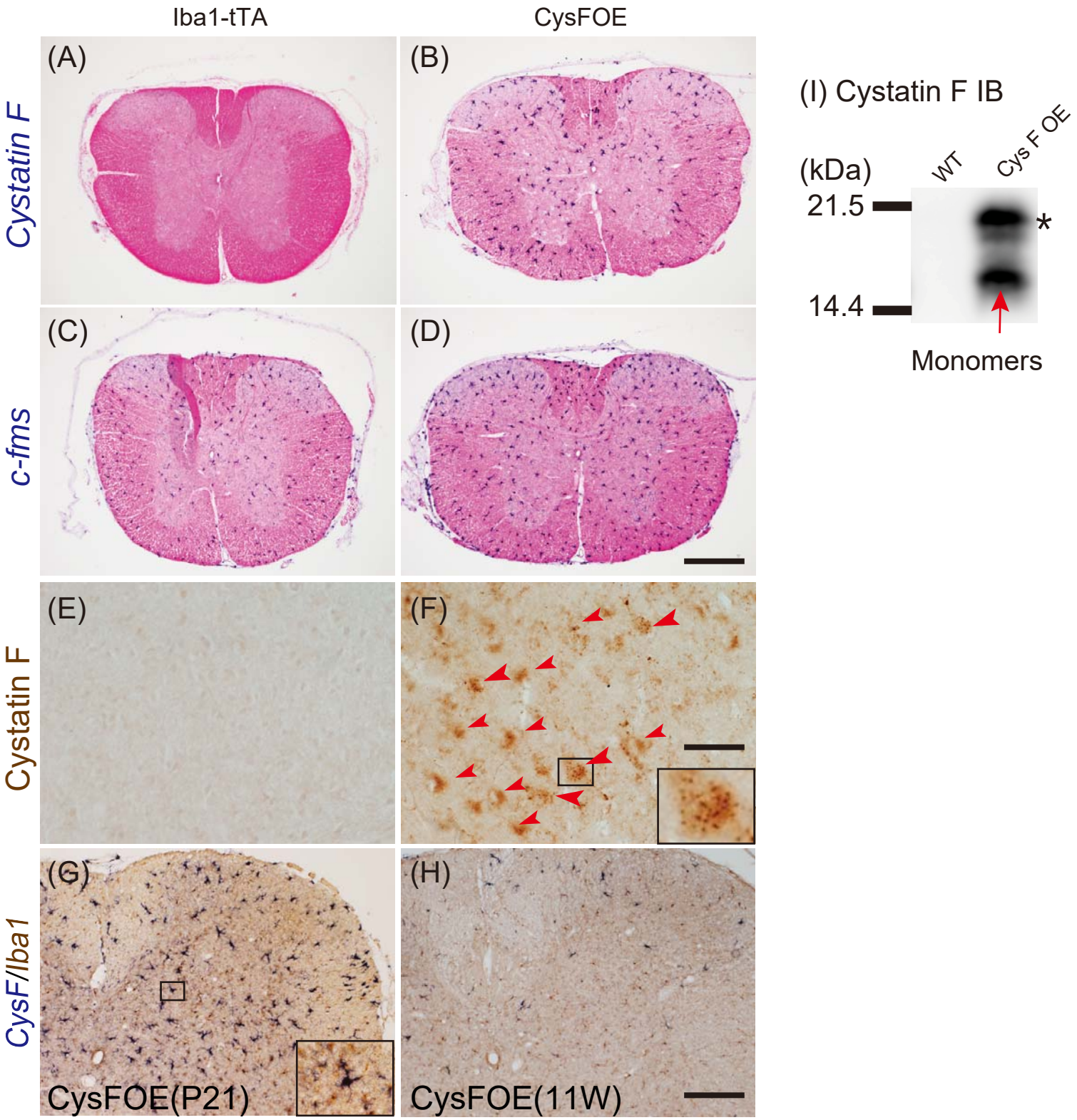
Iba1-tTA
CysFOE
Cystatin F
c-fms
Cystatin F
CysF/Iba1
(A)
(B)
(C)
(D)
(E)
(F)
(G)
(H)
CysFOE(P21)
CysFOE(11W)
(I) Cystatin F IB
(kDa)
WT
Cys F OE
21.5
14.4
*
Monomers

Figure 3

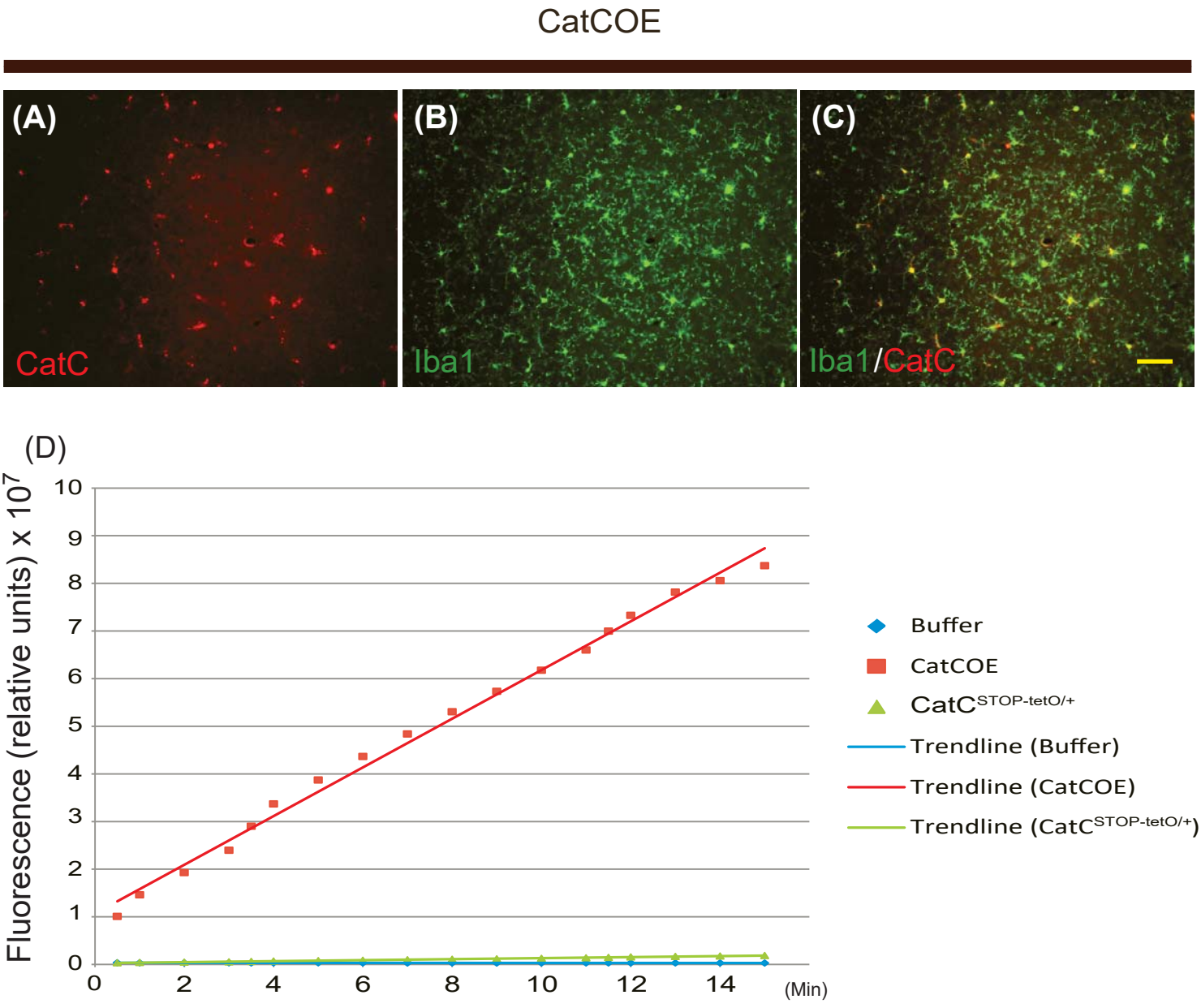
CatCOE
(A)
CatC
(B)
Iba1
(C)
Iba1/CatC
(D)
Fluorescence (relative units) x 10^7
0
1
2
3
4
5
6
7
8
9
10
0
2
4
6
8
10
12
14
(Min)
Buffer
CatCOE
CatC^STOP-tetO/+
Trendline (Buffer)
Trendline (CatCOE)
Trendline (CatC^STOP-tetO/+)

Figure 4

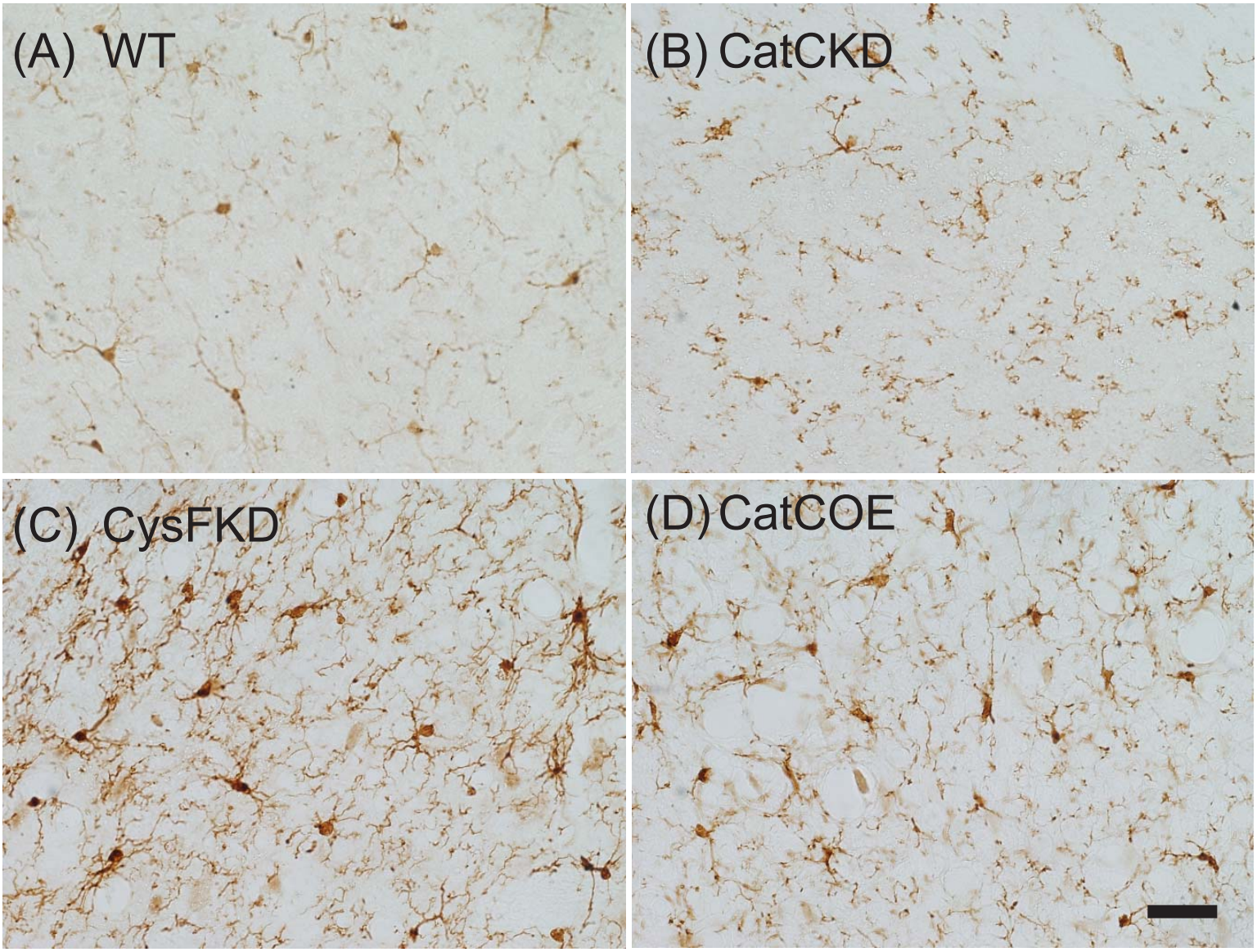

Figure 5

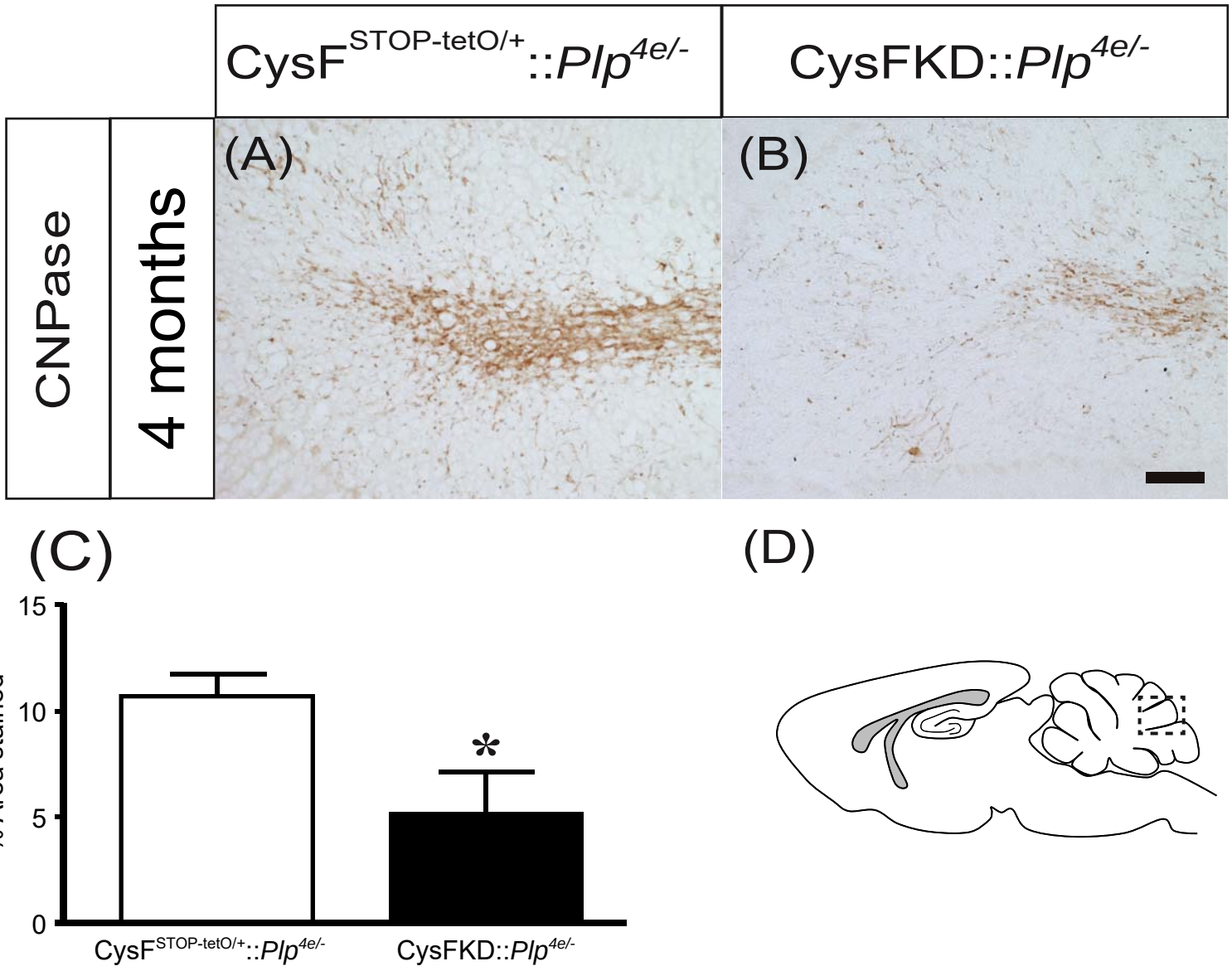
CysF STOP-tetO/+ ::Plp 4e/-
CysFKD::Plp 4e/-
CNPase
4 months
(A)
(B)
(C)
(D)
% Area stained
15
10
5
0
*
CysF STOP-tetO/+ ::Plp 4e/-
CysFKD::Plp 4e/-

Figure 6

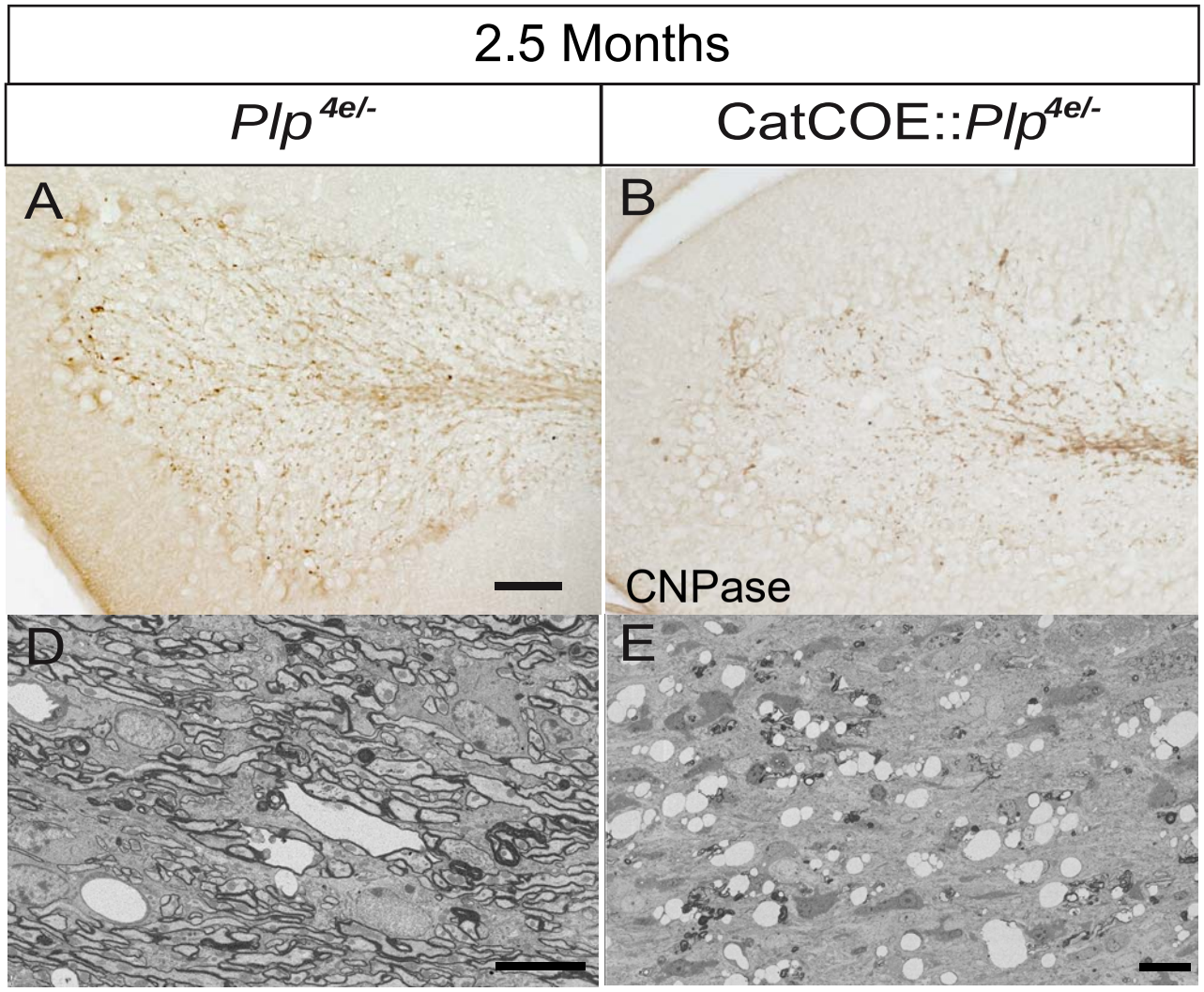
2.5 Months
Plp4e/-
CatCOE::Plp4e/-
A
B
CNPase
D
E

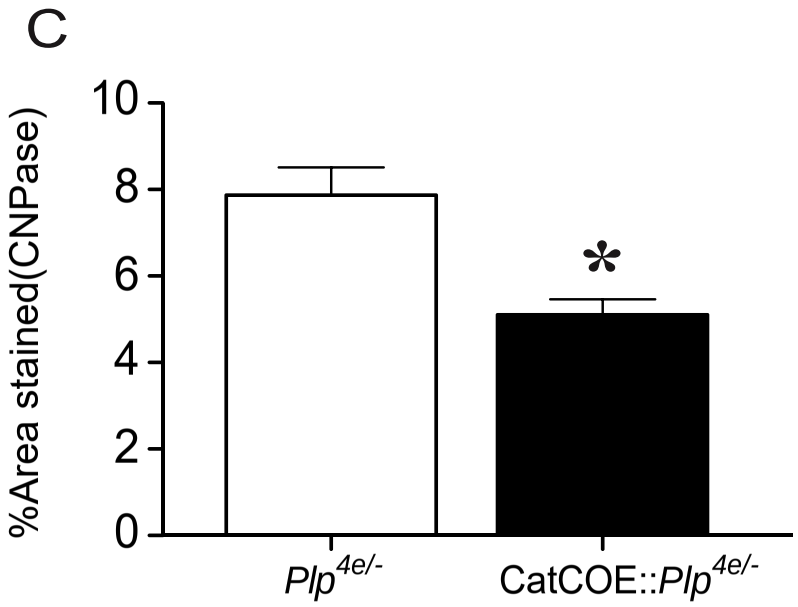
C
%Area stained(CNPase)
10
8
6
4
2
0
*
Plp4e/-
CatCOE::Plp4e/-

Figure 7

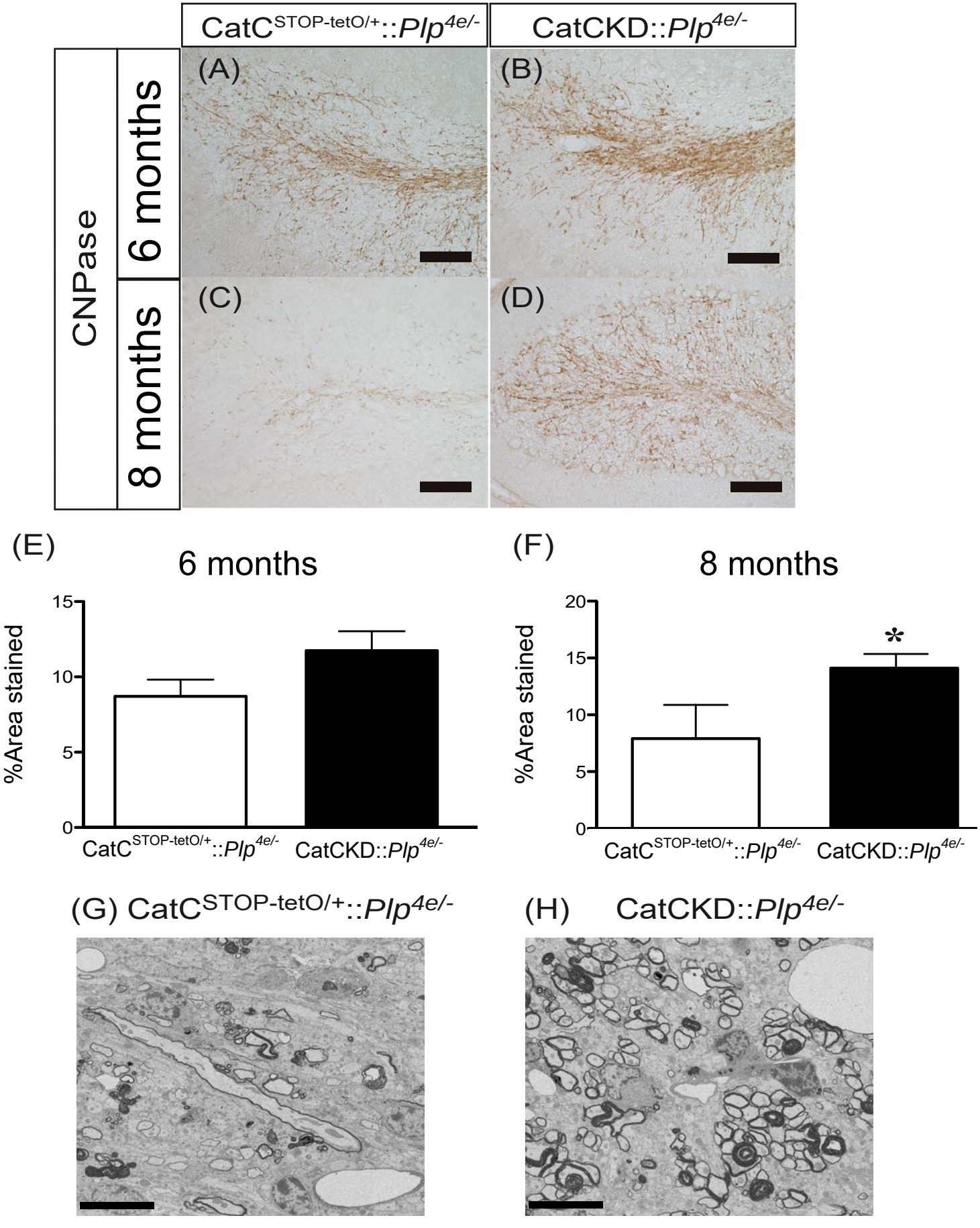
CatC$^{STOP\text{-}tetO/+}$::*Plp*$^{4e/-}$
CatCKD::*Plp*$^{4e/-}$
CNPase
6 months
8 months
(A)
(B)
(C)
(D)
(E)
6 months
%Area stained
15
10
5
0
CatC$^{STOP\text{-}tetO/+}$::*Plp*$^{4e/-}$
CatCKD::*Plp*$^{4e/-}$
(F)
8 months
%Area stained
20
15
10
5
0
*
CatC$^{STOP\text{-}tetO/+}$::*Plp*$^{4e/-}$
CatCKD::*Plp*$^{4e/-}$
(G) CatC$^{STOP\text{-}tetO/+}$::*Plp*$^{4e/-}$
(H) CatCKD::*Plp*$^{4e/-}$

Figure 8

(A)

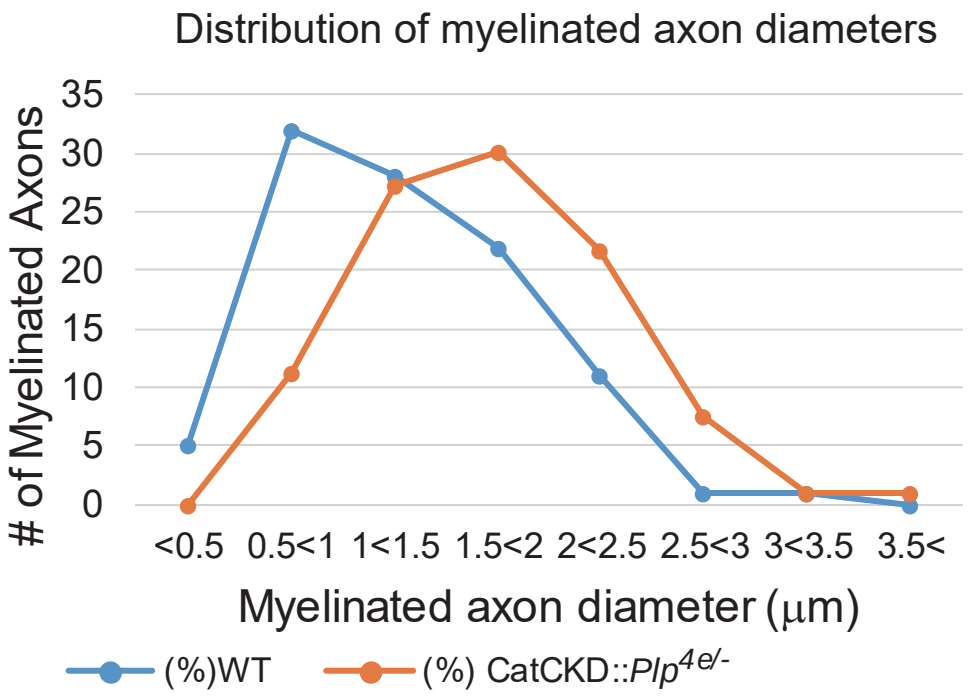
Distribution of myelinated axon diameters
# of Myelinated Axons
35
30
25
20
15
10
5
0
<0.5
0.5<1
1<1.5
1.5<2
2<2.5
2.5<3
3<3.5
3.5<
Myelinated axon diameter (μm)
(%)WT
(%) CatCKD::Plp4e/-

(B)

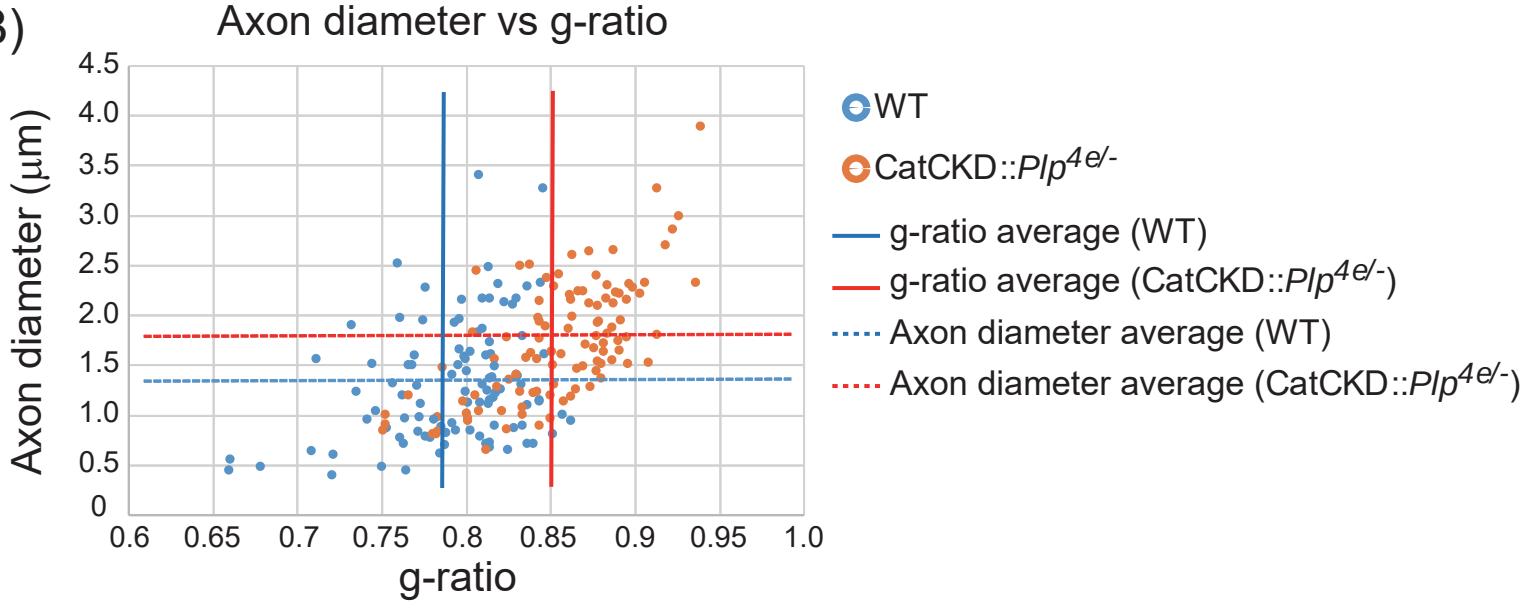
Axon diameter vs g-ratio
Axon diameter (μm)
4.5
4.0
3.5
3.0
2.5
2.0
1.5
1.0
0.5
0
0.6
0.65
0.7
0.75
0.8
0.85
0.9
0.95
1.0
g-ratio
WT
CatCKD::Plp4e/-
g-ratio average (WT)
g-ratio average (CatCKD::Plp4e/-)
Axon diameter average (WT)
Axon diameter average (CatCKD::Plp4e/-)

Figure 9

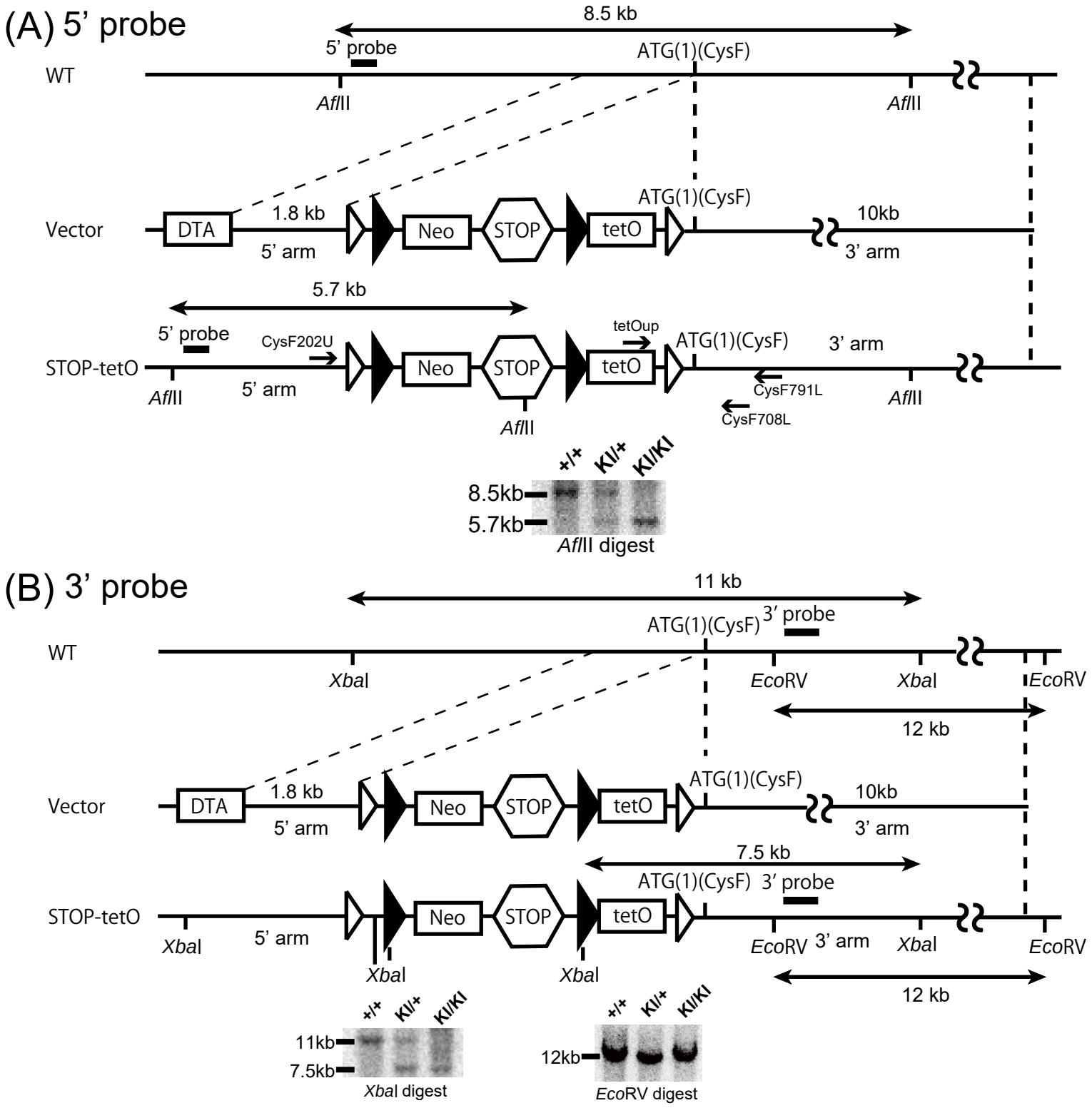
(A) 5' probe
8.5 kb
5' probe
ATG(1)(CysF)
WT
AflII
AflII
Vector
DTA
1.8 kb
5' arm
Neo
STOP
tetO
ATG(1)(CysF)
10kb
3' arm
5.7 kb
5' probe
CysF202U
tetOup
ATG(1)(CysF)
3' arm
STOP-tetO
AflII
5' arm
Neo
STOP
tetO
CysF791L
CysF708L
AflII
AflII
+/+
KI/+
KI/KI
8.5kb
5.7kb
AflII digest
(B) 3' probe
11 kb
ATG(1)(CysF)
3' probe
WT
XbaI
EcoRV
XbaI
EcoRV
12 kb
Vector
DTA
1.8 kb
5' arm
Neo
STOP
tetO
ATG(1)(CysF)
10kb
3' arm
7.5 kb
ATG(1)(CysF)
3' probe
STOP-tetO
XbaI
5' arm
Neo
STOP
tetO
EcoRV
3' arm
XbaI
EcoRV
XbaI
XbaI
12 kb
+/+
KI/+
KI/KI
11kb
7.5kb
XbaI digest
+/+
KI/+
KI/KI
12kb
EcoRV digest

Figure S1

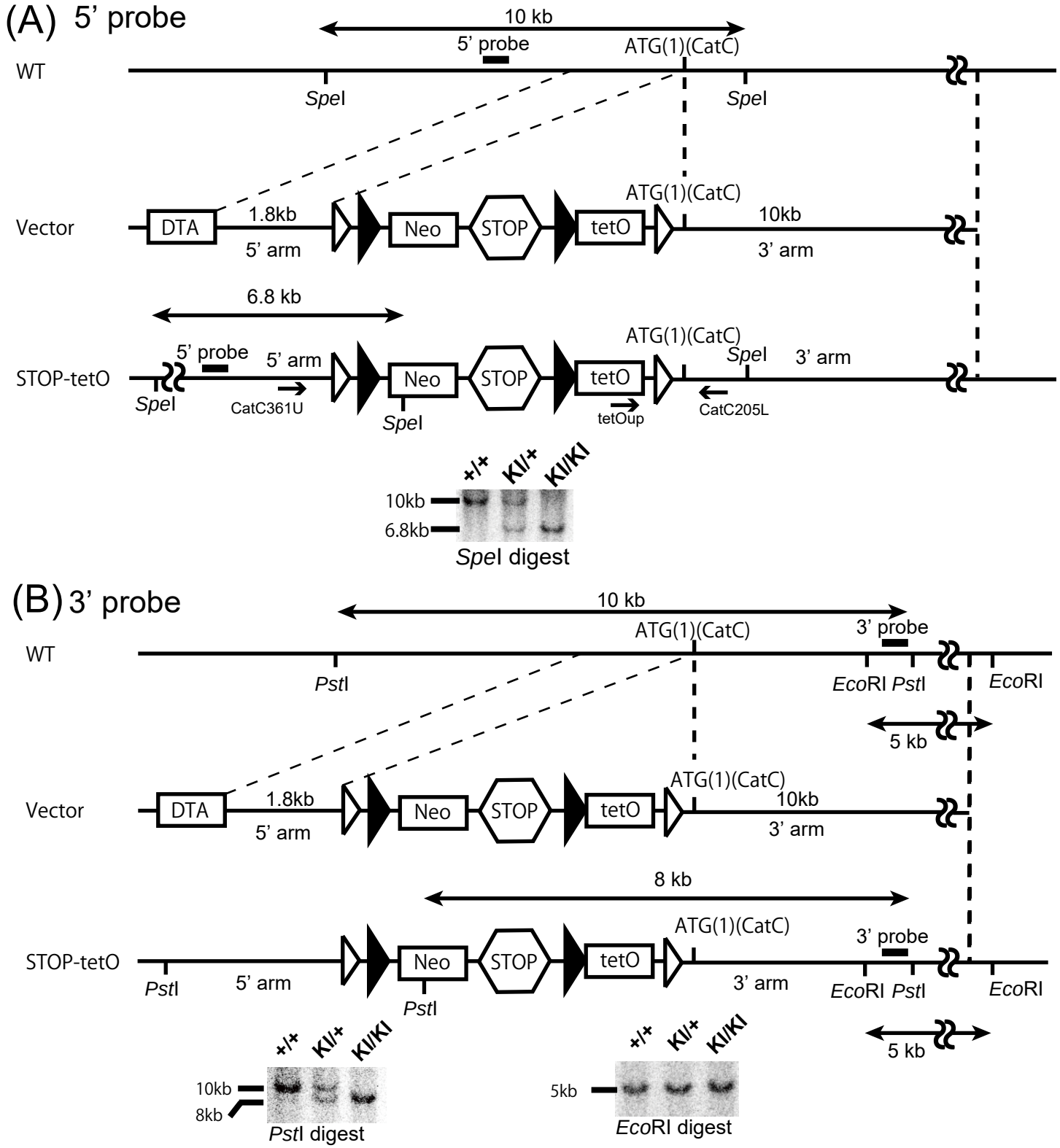
(A) 5' probe
10 kb
5' probe
ATG(1)(CatC)
WT
SpeI
SpeI
Vector
DTA
1.8kb
5' arm
Neo
STOP
tetO
ATG(1)(CatC)
10kb
3' arm
6.8 kb
STOP-tetO
5' probe
5' arm
ATG(1)(CatC)
SpeI
3' arm
SpeI
CatC361U
Neo
STOP
tetO
SpeI
tetOup
CatC205L
+/+
KI/+
KI/KI
10kb
6.8kb
SpeI digest
(B) 3' probe
10 kb
ATG(1)(CatC)
3' probe
WT
PstI
EcoRI PstI
EcoRI
5 kb
Vector
DTA
1.8kb
5' arm
Neo
STOP
tetO
ATG(1)(CatC)
10kb
3' arm
8 kb
STOP-tetO
ATG(1)(CatC)
3' probe
PstI
5' arm
Neo
STOP
tetO
3' arm
EcoRI PstI
EcoRI
PstI
5 kb
+/+
KI/+
KI/KI
10kb
8kb
PstI digest
+/+
KI/+
KI/KI
5kb
EcoRI digest

Figure S2